THE PLASTIC DEFORMATION OF SINTERED IRON

by

N. KRISHNA

Submitted to the Faculty of Science and
Engineering of the University of Ottawa
in partial fulfillment of the requirements
for the degree of

MASTER OF APPLIED SCIENCE

in

MECHANICAL ENGINEERING

Ottawa, Canada

February 1971

ACKNOWLEDGEMENT

The author is deeply indebted to his supervisor, Dr. A. S. Krausz, for the advice, guidance, encouragement and personal understanding throughout the course of this research. He also is indebted to Dr. E. Winkler for his guidance and helpful suggestions during the course of the forging tests. The interest shown by the other faculty members of the Mechanical Engineering Department, particularly Dr. A. Feingold is acknowledged.

The author wishes to express his gratitude to Mr. N. S. Spence, Mr. J. A. Perry, Mr. P. J. Todkill and Mr. J. R. Emmett of the Department of Energy, Mines and Resources for their assistance from time to time.

Author's appreciation is also extended to Mr. G. Toth for his technical assistance. The willing assistance by W. Hofmann, O. Dalnoki and P. Inderbitzin throughout the project is appreciated.

The financial support provided by the Defence Research Board is gratefully acknowledged. Acknowledgements are also due to the Metal Powders Division of Domtar Chemicals Ltd. for their supply of the specimen material.

ABSTRACT

Over the last few years there was a rapid increase in the use of powder metallurgy products. Many of these products are subjected to further cold or hot forming operations. A study was, therefore, carried out to obtain information on the plastic behavior of type M.P. 32 sintered iron. This iron is manufactured by Domtar and is one of the major products among the exported sintered metals.

Stress relaxation tests were carried out at room temperature to obtain information on the stress dependence of the plastic strain rate and on the mechanisms which control the dislocation movement in sintered iron. The experimental results were analyzed with a two term rate theory equation which takes into consideration both the forward and the backward movement of the dislocations. The analysis showed that in the early stage, when the strain rate is high, the behavior can be explained by considering only one mechanism. However, in the low strain rate range a second mechanism had a significant effect on the plastic deformation of sintered iron.

The internal stress was also determined in sintered iron. The measurements were carried out by a combination of stress and strain relaxation tests. The internal stress was found to be $\sim 87\% \pm 6\%$ of the applied stress. Tensile test results obtained over a strain rate range of 0.001/min to 1.0/min, indicated that there was no consistent dependence of the stress-strain characteristics on the strain rate at the investigated experimental conditions. This behavior is in full agreement with the conclusions drawn from the internal stress measurements.

TABLE OF CONTENTS

LIST OF TABLES

LIST OF FIGURES

FIGURE PAGE

NOMENCLATURE

A = Pre-exponential factor in the rate equation

b = Burgers vector

d = Distance covered by the dislocations to overcome the energy barrier

E = Elastic modulus

E' = Combined elastic modulus

ΔE = Apparent activation energy

$\Delta E^{\neq}$ = Activation energy

k = Boltzmann constant

m = Slope of the $\log \sigma_a$ vs $\log (-\Delta \dot{\sigma})$ relation

N = Total number of particles in a system

N_i = Number of particles at the energy level $\Delta \epsilon_i$

n = $V/2\,kT$

S = Burgers vector times the length of the dislocation between two barriers

Str = Structure

T = Absolute temperature

t = Time

V = Activation volume

v = Average dislocation velocity

V_o = Constant in the equation $V = V_o(\tau_a / \tau_o)^m$

Greek letters

α = Geometrical factor in Orowan's equation

$\Delta\epsilon_i$ = Energy level of the particles

$\overline{\Delta\epsilon}$ = Average energy of the particles

ϵ = Tensile strain

ϵ_a = Strain of the specimen due to the deformation of the test jig and load cell

ϵ_e = Elastic strain

ϵ_p = Plastic strain

ϵ_t = Total strain of the specimen during stress relaxation

γ = Shear strain

ℓ = Distance covered by the dislocation after each jump over the energy barrier.

ν = Vibrational frequency of the dislocation line

ρ_m = Mobile dislocation density

σ = Tensile stress

σ_a = Applied tensile stress

σ_{eff} = Effective tensile stress

σ_i = Internal tensile stress

τ = Shear stress

τ_a = Applied shear stress

τ_{eff} = Effective shear stress

τ_i = Internal shear stress

τ_o = Constant in the equation $V = V_o(\tau_a / \tau_o)^m$

Subscripts

b = Denotes the backward movement of the dislocations

f = Denotes the forward movement of the dislocations

1. INTRODUCTION

In modern industry powder metallurgy (P/M) occupies a place of increasing importance (1, 2). It is a manufacturing process for the production of machine parts from fine powders of metals and metallic compounds. Using this method, alloys can be manufactured with compositions which cannot be produced by solidification. High melting point metals and alloys can be shaped, without melting, by sintering below their melting point. Special properties, such as the porous structure of self-lubricating bearings, can be obtained by powder metallurgy. Precision machine components can be fabricated by P/M more economically than by any other method if large quantities of high strength iron, steel or nickel component is needed (3). Although the importance of sintered metals is understated if only the quantity in use is considered, it is of interest to note that while 10 years ago the American automobiles contained ~ 4 lbs of P/M components, they have today ~ 8-9 lbs of sintered components.

Not infrequently, P/M products are subjected to further fabrication either by cold (4) or hot forming. The plastic behaviour during these forming processes is of great interest in the analysis of the manufacturing forces and production rates. Because P/M is a relatively new method, very little relevant information is available.

Iron powder, for sintering, is a multimillion dollar export product of the Canadian industry. The Domtar M. P-32 type powder metallurgy iron has a major share of this. In the present study some of the plastic properties of the sintered M. P. 32 type iron, supplied by Domtar, were investigated.

PLASTIC DEFORMATION IN CRYSTALLINE MATERIALS

Plastic deformation is controlled by four major variables, the shear stress τ, the shear strain rate $\dot{\gamma}$, the temperature T and the structure. The deformation process is fully known if their interrelation

$$f(\tau, \dot{\gamma}, T, Str) = 0 \qquad (1.1)$$

is known over the range of interest. The establishment of this relation is essentially the ultimate purpose of any structural study of plasticity. In principle, relation (1.1) provides the information necessary for the analysis of the stress and strain field.

To determine Eqn. (1.1), it is necessary to take into consideration that plastic deformation occurs by one atomic plane gliding over another in a definite crystallographic direction. This slip does not occur as a rigid body translation but by the discrete movement of rows of atoms moving by one lattice distance in succession. This process requires several orders less energy than the rigid body glide. This stepwise glide process occurs by the movement of line imperfections - dislocations.

In an ideal crystal, the atoms are arranged in a perfect geometrical order. In a real crystal, however, some of the atoms are always out of register. The imperfection in which a line, or row, of atoms is out of register is of particular interest in the study of plastic deformation of crystals. A line imperfection - dislocation - is shown in Fig. 1.1. Although physically incorrect, it is instructive to consider that a dislocation can be considered to be produced by a stress applied to a perfect crystal as shown in Fig. 1.1. After a dislocation has been created, it moves under the effect of the shear stress. As the figure shows, bonds are broken among rows of atoms as the dislocation moves across the

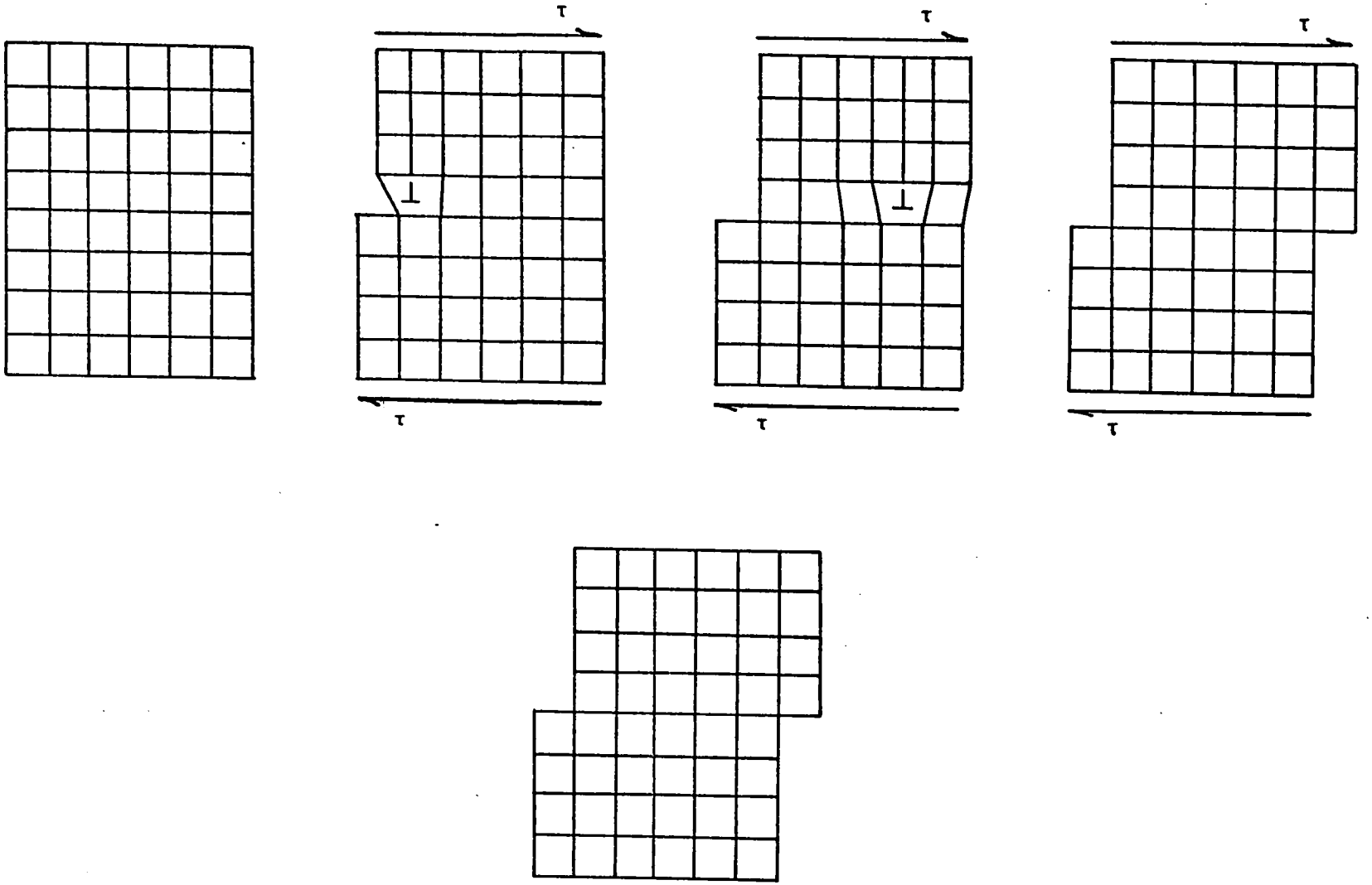

Fig. 1.1 The diagram illustrates the generation and motion of a dislocation(⊥) across a lattice under the effect of a shear stress τ

crystal and new bonds are established resulting in a permanent shape change. This is the physical process of plastic deformation.

The breaking and reestablishing of bonds associated with the movement of dislocations is necessarily a discontinuous process.

Under the effect of the shear stress, the dislocation moves at a high velocity until it encounters an obstacle with a high enough energy to stop it. An obstacle is essentially an atomic configuration where the rearrangement of bonds, due to the movement of the dislocation, is associated with an energy greater than the work that can be performed by the stress acting on the dislocation.

Fig. 1.2 shows the energy field encountered by the dislocation ($\perp$) as it moves across the crystal. The energy level ΔE_W corresponding to the work performed by the stress is high enough to carry the dislocation over the periodic potential energy field of the crystal. The dislocation is stopped, however, at the barrier where the energy level is higher than ΔE_W.

The rearrangement of the atoms, which corresponds to the dislocation overcoming the energy barrier, can occur only when the atoms acquire enough energy corresponding to the activated state $\neq$. When the energy level of the atoms is $\Delta E^{\neq}$, the dislocation can move over the barrier and is free to move again at a high velocity until it encounters another barrier. The energy difference $\Delta E^{\neq} - \Delta E_W$ necessary for this process is supplied by the thermal energy of the crystal. The movement of the dislocation is, therefore, a thermally activated process. Because the waiting time in front of the barrier is large, compared to the time needed to move between the barriers, the average dislocation velocity is determined by the waiting time which in turn depends on the rate of

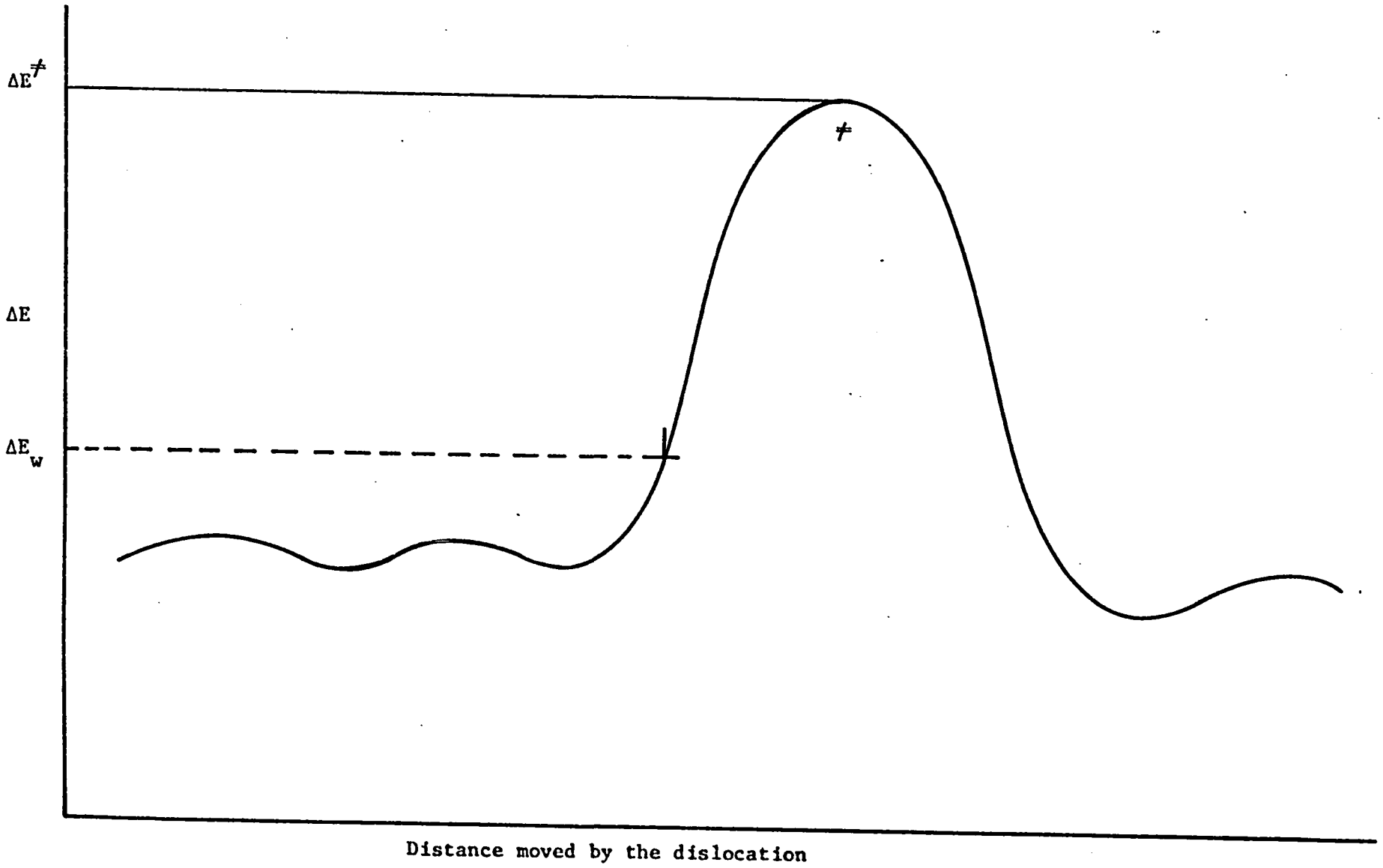

Fig. 1.2 Diagram showing the energy field encountered by the dislocation.

the fluctuation of the thermal energy. In consequence the dislocation mobility is controlled by the thermally activated process of overcoming the energy barrier.

Because the dislocation velocity is controlled by thermal activation and is affected by the stress

$$v = v(\tau, T, Str)$$

The relation between the strain rate $\dot{\gamma}$ and the stress, temperature and structure is expressed by Orowan's (5) equation.

$$\dot{\gamma} = a\ b\ \rho_m\ v(\tau, T, Str) \qquad (1.2)$$

In this expression, a is a geometrical factor, b is the Burger's vector and ρ_m is the mobile dislocation density.

Eqn. (1.2) fully describes the plastic deformation of crystalline materials. It is the final aim of the structural study of plasticity to determine Eqn. (1.2). This is then to a major extent a study of the dislocation velocity.

Johnston and Gilman (6) studied the effect of stress on dislocation velocity in LiF by etch-pit technique. To describe the experimental results, they used the purely empirical engineering relation

$$v = v_o\ (\tau_a/\tau_o)^m \quad \text{where}$$

τ_a is the applied shear stress and v_o, τ_o and m are constants for a particular condition of testing. Becker (7) first suggested that in plastic deformation, the thermal fluctuations assisted the applied stress in overcoming the energy barriers. He described plastic deformation by

the semi-empirical Arrhenius equation

$$v = \nu l \exp\left[-\Delta E\,(\tau_{eff}) / kT\right]$$

where ν = the frequency term

l = distance covered by the dislocation after each activation

τ_{eff} = the effective shear stress acting on the dislocation. It is the resultant of the applied shear stress τ_a and the internal stress τ_i

$$\tau_{eff} = \tau_a - \tau_i$$

ΔE = the apparent activation energy which decreases with increasing effective shear stress τ_{eff}.

T = the absolute temperature

k = the Boltzmann constant.

The equation suggested by Becker is semi-empirical, however, and for a better understanding of the plastic deformation process, the dislocation velocity should be described by an equation derived from basic principles. Because the movement of dislocations is always associated with the breaking and reestablishing of bonds between the atoms, the thermally activated plastic deformation process is identical with the chemical reactions. Consequently, the study of plastic flow is part of chemical kinetics and the process is described by the rate theory. The derivation of an equation for the dislocation velocity is therefore based essentially on the rate theory.

DERIVATION OF THE RATE EQUATION (8, 9)

Consider a system of N particles with a total energy ΔE having N_i particles at the energy level $\Delta\epsilon_i$ where $\sum_{i=o}^{\infty} N_i = N$ and

$\sum_{i=o}^{\infty} N_i \Delta\epsilon_i = \Delta E$. In this system, the energy difference between successive energy levels is considered equal. There are many ways of distributing the particles at the different energy levels with constant N and ΔE. The most probable distribution corresponds to the equilibrium state of the system. In other words, the equilibrium distribution is that which can be formed in a maximum number of ways without changing the number of particles at each energy level.

To determine the equilibrium distribution, first consider the energy levels to be empty. Fill the energy levels with the particles, one by one, beginning from $\Delta\epsilon_o$. There are N ways of selecting the first particle and (N-1) for the second particle. The number of ways in which the first two particles can be selected is $\frac{N(N-1)}{2}$ because the order of selection is immaterial. Similarly proceeding, the number of ways of selecting N_o particles to fill the energy level $\Delta\epsilon_o$ is $N!/((N-N_o)!N_o!)$ Of the remaining $(N-N_o)$ particles, the energy level $\Delta\epsilon_1$ can be filled in $(N-N_o)!/((N-N_o-N_1)!N_1!)$ number of ways. Continuing this way, the total number of ways of selecting N particles to fill in all the energy levels is $W = N!/(N_o!N_1!N_2!..)$. W should be maximum for the equilibrium distribution. Thus small changes in N_i should have minimum effect on W for the equilibrium distribution. To bring about a small change in N_i, two particles are removed from the energy level $\Delta\epsilon_r$ and one is inserted into $\Delta\epsilon_{r+1}$ and the other into $\Delta\epsilon_{r-1}$. This will cause a change δW in the number of possible ways of distributing the particles. Thus,

$$\delta W = (N!/(N_o!N_1!N_2!....N_{r-1}!N_r!N_{r+1}!....))$$

$$- (N!/(N_o!N_1!N_2!....(N_{r-1}+1)!(N_r-2)!(N_{r+1}+1)!....))$$

where $\Delta\epsilon_{r+1} - \Delta\epsilon_r = \Delta\epsilon_r - \Delta\epsilon_{r-1}$ (1.3)

Hence $N_{r-1}!\, N_r!\, N_{r+1}! = (N_{r-1}+1)!\,(N_r-2)!\,(N_{r+1}+1)!$

$$N_r(N_r-1) = (N_{r-1}+1)(N_{r+1}+1)$$

and when N_{r-1}, N_r and N_{r+1} are large numbers,

$$N_r^2 \approx N_{r-1}\, N_{r+1}$$

$$2 \log N_r \approx \log N_{r-1} + \log N_{r+1}$$

$$\log N_{r+1} - \log N_r \approx \log N_r - \log N_{r-1} \qquad (1.4)$$

Eqns(1.3)and(1.4)will be simultaneously satisfied if the logarithm of the number of particles is proportional to the corresponding energy level. The relation between them can be represented by an equation of the form,

$$N_i = B \exp(\mu \Delta\epsilon_i)$$

where B is the proportionality constant.

To determine μ, consider two independent systems in thermal contact. The systems are denoted by superscripts p and q. In thermal equilibrium, the product $W^p W^q$ is a maximum. Move a particle in the first system from $\Delta\epsilon_a^p$ to $\Delta\epsilon_b^p$ and one in the second system from $\Delta\epsilon_x^q$ to $\Delta\epsilon_y^q$ where,

$$\Delta\epsilon_a^p - \Delta\epsilon_b^p = \Delta\epsilon_y^q - \Delta\epsilon_x^q$$

thus conserving the total energy and the number of particles. Equating

$W^p W^q$ before and after the change, it can be shown that $\mu^p = \mu^q$. Hence μ must be the same for all systems in thermal equilibrium.

It is thus sufficient to determine μ for one simple system. Consider an ideal gas at temperature T. The average energy of the particles is

$$\overline{\Delta\epsilon} = \frac{\text{Total energy of the system}}{\text{Total number of particles}}$$

$$= \sum_{i=o}^{\infty} N_i \, \Delta\epsilon_i \Big/ \sum_{i=o}^{\infty} N_i$$

$$= \frac{\sum_{i=o}^{\infty} \Delta\epsilon_i \, B \exp(\mu \Delta\epsilon_i)}{\sum_{i=o}^{\infty} B \exp(\mu \Delta\epsilon_i)}$$

$$= \frac{\sum_{i=o}^{\infty} \Delta\epsilon_i \exp(\mu \Delta\epsilon_i)}{\sum_{i=o}^{\infty} \exp(\mu \Delta\epsilon_i)}$$

For the one dimensional case, writing $\Delta\epsilon_i = m v_i^2 / 2$ where m is the mass and v_i the velocity of the particles and replacing the summation, by integration, one gets

$$\overline{\Delta\epsilon} = \frac{\int_{-\infty}^{\infty} \frac{1}{2} m v^2 \exp(\mu m v^2/2) \, dv}{\int_{-\infty}^{\infty} \exp(\mu m v^2/2) \, dv}$$

$$= -\frac{1}{2\mu}$$

From the kinetic theory of gases, the average energy of the particles for each degree of freedom is given by

$$\overline{\Delta\epsilon} = \frac{1}{2} \, kT \qquad \text{where}$$

k is the Boltzmann constant.

Comparing the above two expressions, we find that

$$\mu = - \frac{1}{kT}$$

The equation for the energy distribution of a system in equilibrium becomes,

$$\frac{N_j}{N} = \frac{\exp(-\Delta\epsilon_j/kT)}{\sum_{i=o}^{\infty} \exp(-\Delta\epsilon_i/kT)}$$

The ratio of the number of dislocations at the activated state $N^{\neq}$ to the total number of dislocations N at or above the initial state is

$$\frac{N^{\neq}}{N} = \frac{\sum_{i=o}^{\infty} \exp\left[-(\Delta\epsilon^{\neq} + \Delta\epsilon_i)/kT\right]}{\sum_{i=o}^{\infty} \exp(-\Delta\epsilon_i/kT)}$$

$$= \exp(-\Delta\epsilon_i/kT)$$

Now consider the energy map for the dislocation motion given by Fig. 1.3. The dislocations can move in either direction. Let P and Q denote the initial positions in front of an obstacle for the dislocations moving in the forward and reverse directions respectively. The height of the energy barrier is $\Delta E_f^{\neq}$ and $\Delta E_b^{\neq}$ for the forward and reverse movement of the dislocations respectively.

If a shear stress τ_{eff} is applied, the energy barrier would change

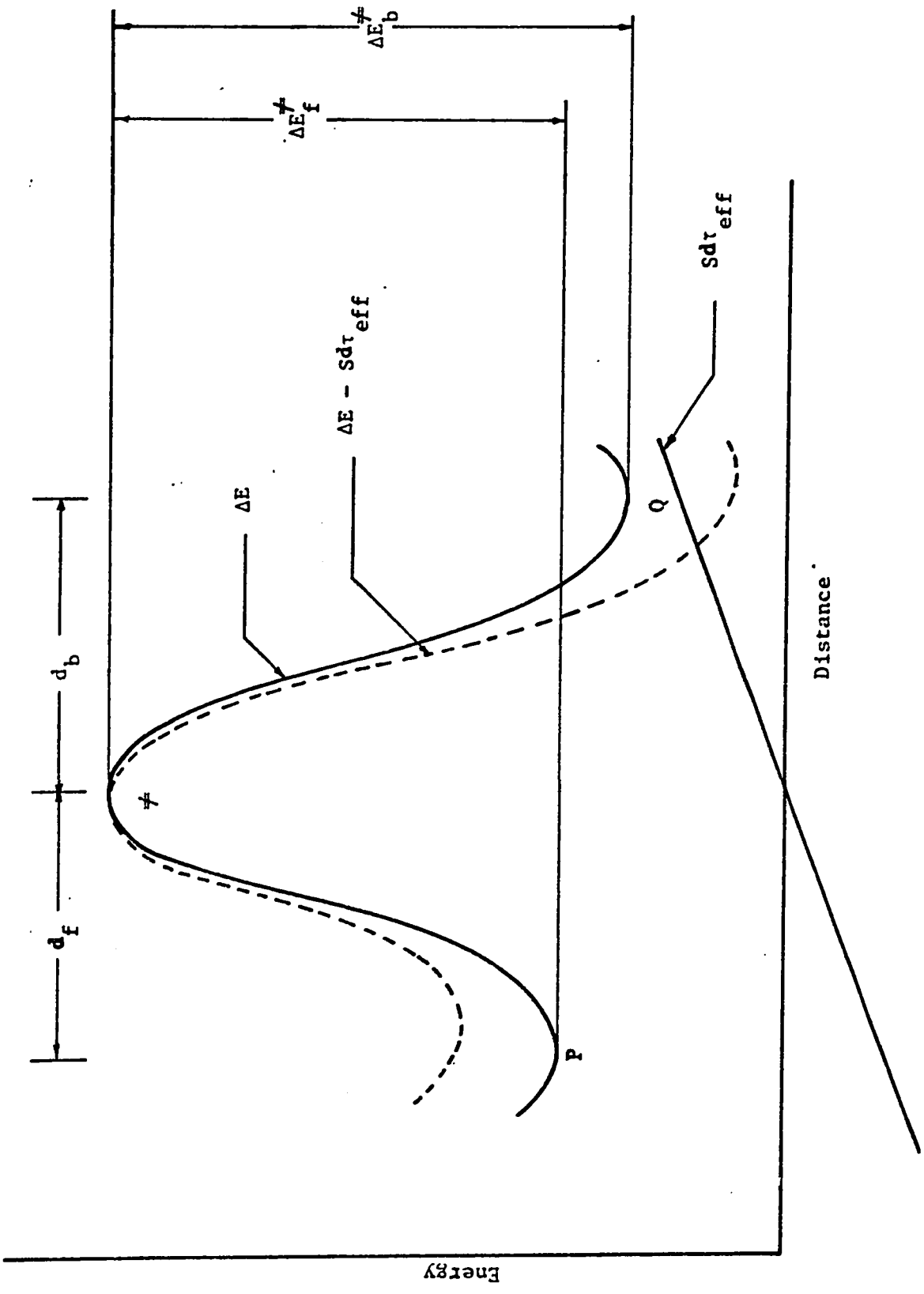

Fig. 1.3 The diagram illustrates the energy barrier encountered by the dislocation.

as shown by the dotted curve in Fig. 1.3. The height of the energy barrier will be reduced by the work done by the shear stress. Because the stress is acting in the forward direction, the height of the barrier will be reduced by $(S_f d_f \tau_{eff})$ in the forward direction and increased by $(S_b d_b \tau_{eff})$ in the reverse direction, where S is the Burgers vector times the length of the dislocation between two barriers, d_f and d_b are the distance covered by the dislocations to overcome the energy barrier in the forward and reverse direction respectively. Thus the height of the energy barrier will be $(\Delta E_f^{\neq} - S_f d_f \tau_{eff})$ in the forward direction and $(\Delta E_b^{\neq} + S_b d_b \tau_{eff})$ in the reverse direction. $S d$ is the activation volume V.

The velocity v of the dislocations will be given by the probability of finding the dislocations at or above the energy level $\Delta E^{\neq}$ multiplied by the vibrational frequency of the dislocation line ν, times the distance ℓ covered after each jump over the energy barrier. Considering the forward and reverse movement of the dislocations, the net velocity in the forward direction under the effect of the effective stress τ_{eff} is

$$v = v_f - v_b = \nu \ell_f \exp\left(-(\Delta E_f^{\neq} - V_f \tau_{eff})/kT\right)$$

$$- \nu \ell_b \exp\left(-(\Delta E_b^{\neq} + V_b \tau_{eff})/kT\right)$$

where subscripts f and b denote the forward and reverse movement of the dislocations respectively. Investigations showed that the equation is a good representation of the dislocation velocity for a wide range of metallic and non-metallic crystals (10)

VARIOUS METHODS OF DETERMINING THE STRESS DEPENDENCE OF DISLOCATION VELOCITY.

The most reliable method of measuring the stress dependence of the dislocation velocity is by direct observation using the etch-pit technique. However, this method cannot be applied to many metals and indirect means of measuring the dislocation velocity were developed.

Many attempts have been made to develop indirect methods. These methods utilize Orowan's equation

$$\dot{\gamma} = a\, b\, \rho_m\, v$$

Because only the product $\rho_m v$ can be determined by these testing methods, the stress dependence of the dislocation velocity can only be measured if the mobile dislocation density ρ_m remains constant. The three most common test types are: (11)

1. The strain rate change experiments,
2. The discrete stress change experiments,

and 3. The stress relaxation tests.

Strain rate change experiments

In these experiments, the specimen is deformed at constant strain rate $\dot{\gamma}_1$ and at some stage, the strain rate is changed instantaneously to $\dot{\gamma}_2$. The corresponding stress change $\Delta\tau$ is measured as shown in Fig. 1.4. The relation between $\Delta\tau$ and $\dot{\gamma}$ is given by (11)

$$\Delta\tau = \frac{kT}{V}\, \Delta \ln \dot{\gamma} = \frac{kT}{V}\, \ln \frac{\dot{\gamma}_2}{\dot{\gamma}_1}$$

from which the activation volume V is determined. This is in agreement with the rate theory when the effect of the backward movement of dislocations is negligible.

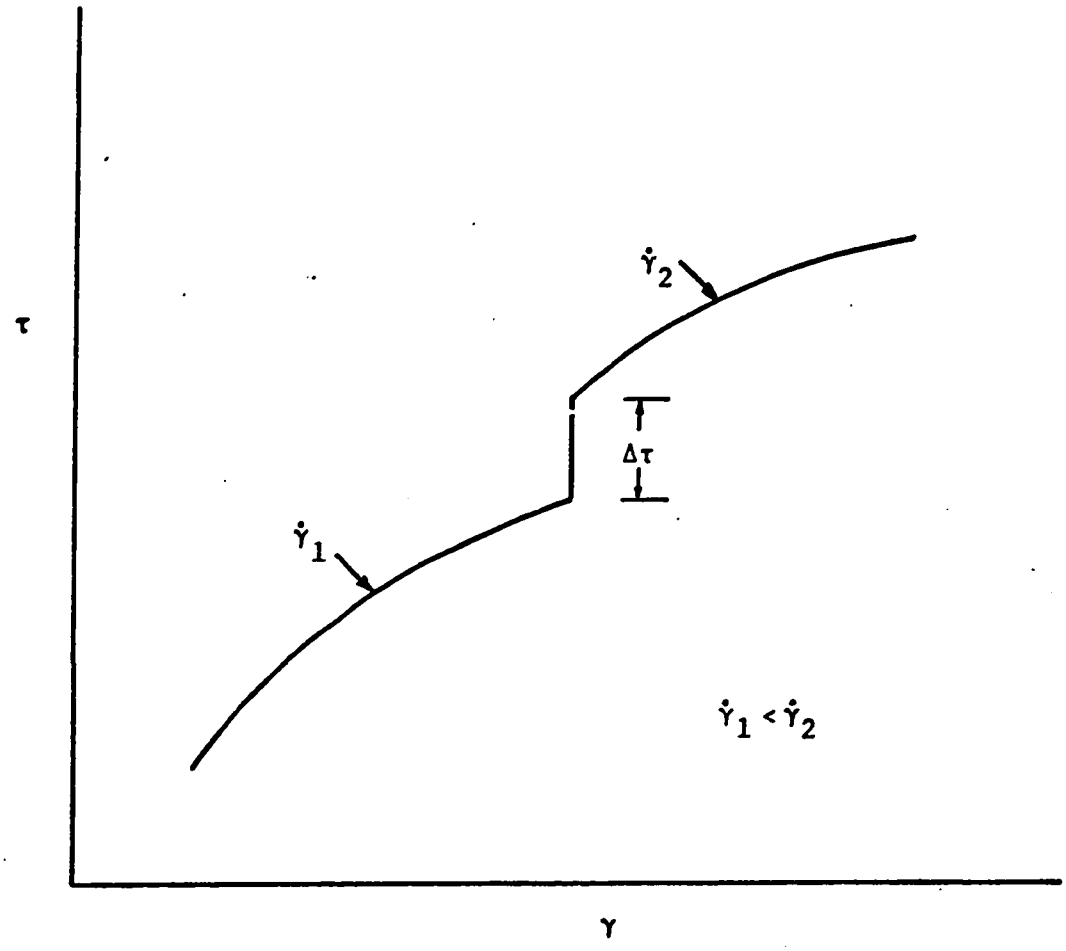

Fig. 1.4 The figure illustrates the variables associated with the strain rate change experiment.

Discrete stress change experiments

These experiments are essentially constant stress creep tests (Fig. 1.5) in which at time 't' the stress is instantaneously increased and maintained constant and the specimen allowed to creep further. Wyatt(12) found that the creep curve B obtained after the stress increment could be matched to the creep curve A obtained before the increment by making a suitable time shift Δt. Wyatt also found a linear relationship between the stress change ($\Delta \tau$) and the logarithm of the time shift ($\Delta \log t$) (Figs 1.6, 1.7). Cottrell(13) showed that the activation volume V can be measured from the above experiment by using the relation

$$\frac{d \ln t}{d\tau} = - \frac{V}{kT}$$

in agreement with the rate theory when the effect of the backward movement of the dislocations is negligible.

Stress relaxation test

This method of testing is used in the present investigation and is explained in detail in the next section.

STRESS RELAXATION TEST

It was one of the purposes of the present investigation to obtain some information on the stress dependence of dislocation velocity in sintered iron. To achieve this, the temperature and structure of the specimen should be constant during the test. Hence stress relaxation tests were carried out at constant temperature.

Ideally, the experimental method consists of loading the specimen to the desired stress level and then keeping its length constant,

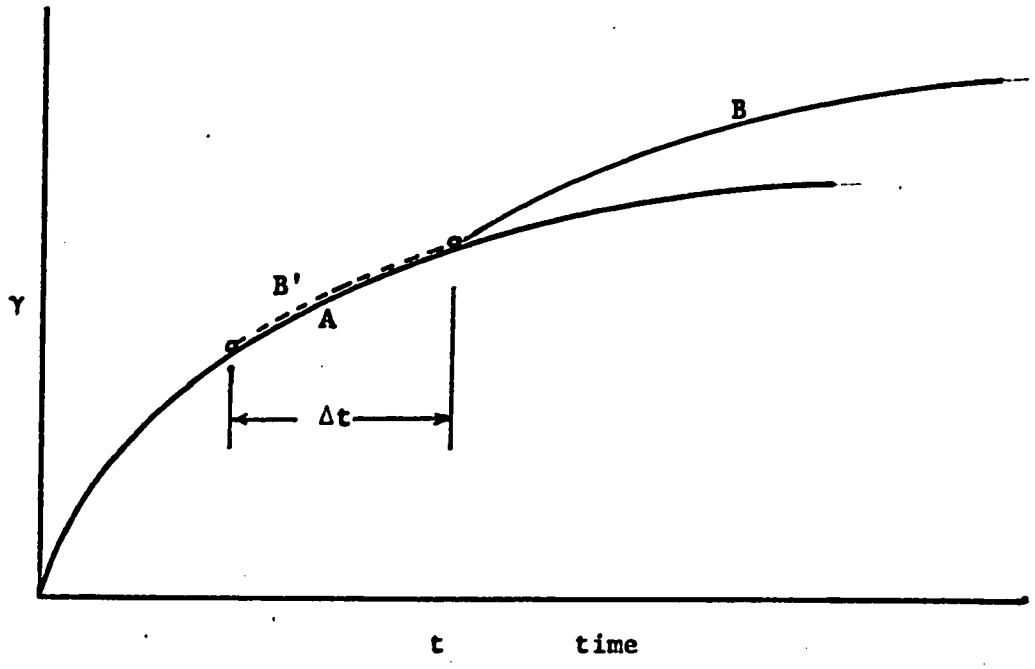

Fig. 1.5

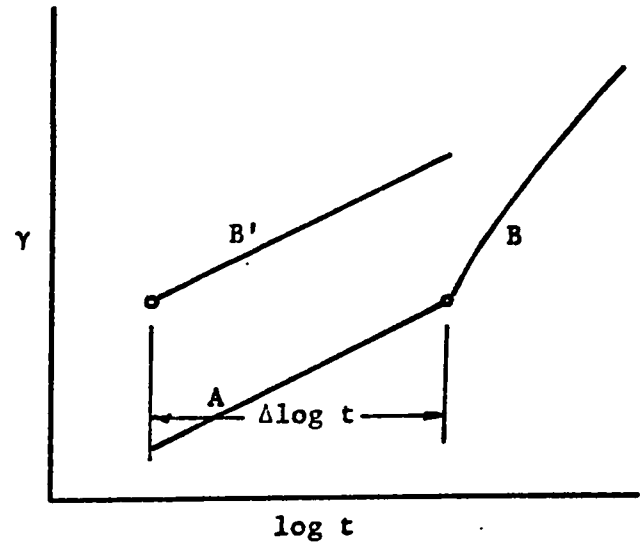

Fig. 1.6

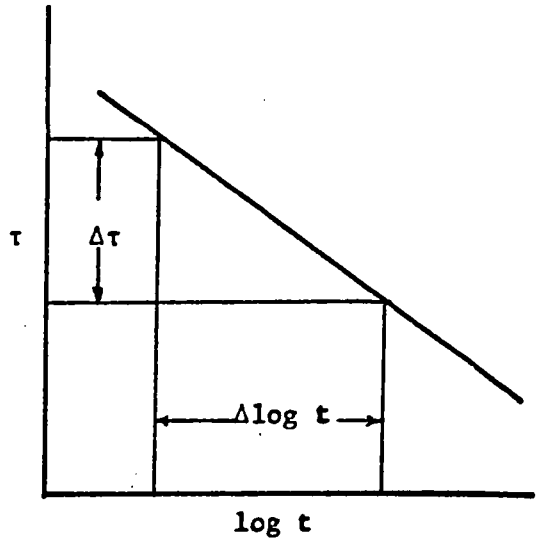

Fig. 1.7

Figs. 1.5 to 1.7 The figures illustrate the variables associated with the discrete stress change experiment.

so that during stress relaxation, the total strain ϵ_t of the specimen is zero. Under the effect of the stress, the specimen deforms plastically. However, because the specimen is restrained from elongation, an elastic strain ϵ_e equal in magnitude but opposite in sign to the plastic strain ϵ_p is produced and the stress relaxes (Fig. 1.8). Thus,

$$\epsilon_t = \epsilon_p + \epsilon_e = 0$$

$$\epsilon_p = - \epsilon_e$$

Therefore, the decrease in stress is equal to $E\ \epsilon_e$ where E is the elastic modulus of the specimen (Fig. 1.9 a).

The ideal condition cannot be achieved because the test jig and load cell deform while the load decreases. Therefore during the experiment, a continuous change in the length of the specimen does occur. This change is equal to the total deformation of the test jig and the load cell when the load decreases (Fig. 1.9 b). Hence,

$$\epsilon_t = \epsilon_a = \epsilon_p + \epsilon_e$$

$$\epsilon_p = \epsilon_a - \epsilon_e$$

and the decrease in stress is equal to $E'(\epsilon_a - \epsilon_e)$ where ϵ_a is the strain of the specimen due to the deformation of the load cell and test jig and E' is the combined elastic modulus of the test jig, load cell and the specimen (14).

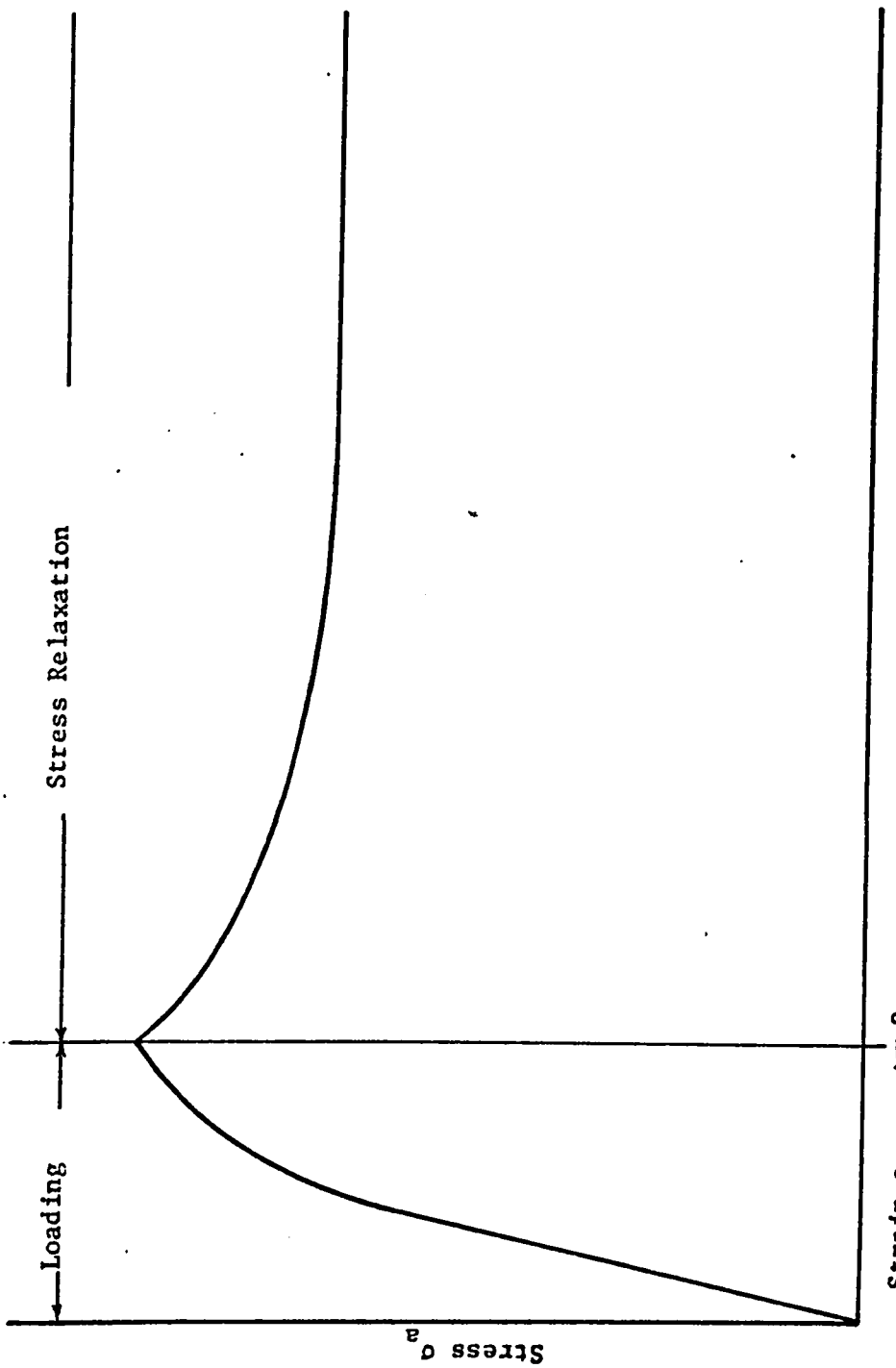

Fig. 1.8 The figure shows the stress relaxation test.

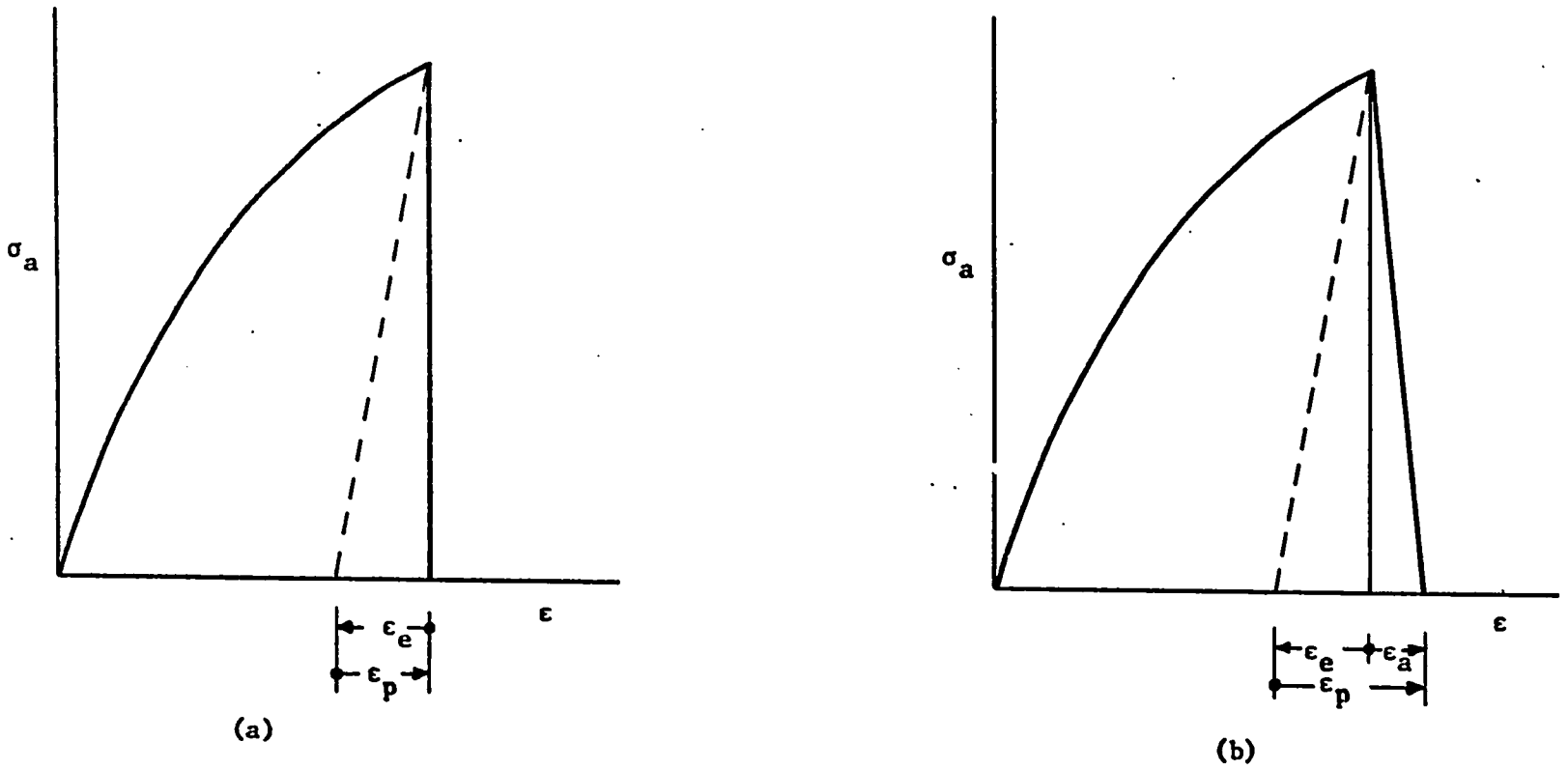

ε_p = Plastic strain of the specimen.

ε_e = Elastic strain of the specimen.

ε_a = Strain of the specimen due to the deformation of the test jig and load cell.

Fig. 1.9 The figures illustrate a) the ideal stress relaxation process and b) the experimental stress relaxation process.

REVIEW ON STRESS RELAXATION TESTS

The earliest stress relaxation tests were carried out by Trouton and Rankine (15) on Pb in 1904. They approximated the ideal stress relaxation by maintaining the length of the specimen within two limits. This was accomplished by removing part of the weight hanging on the specimen when the elongation limit was reached to bring the length of the specimen back to the lower limit. Boyd (16) improved on this method in his stress relaxation tests by having a relay controlled system which automatically maintained the length of the specimen to within $\pm$ 1/75,000 of an inch over a gage length of 20 in.

The complexity of maintaining the length of the specimen within close limits by the above methods led to another method in which a small continuous change in the length of the specimen is allowed during stress relaxation. The change in the length of the specimen depends on the rigidity of the testing system and consequently very rigid machines are preferred in this method.

Feltham(17, 18)carried out stress relaxation tests on α-Brass and Mg on a Hounsfield Tensometer. Most of the investigations were carried out on the Instron type machines. Using these machines stress relaxation was studied by Sargent (19) in Nb, Sargent and Shaw (20) in Mo, Wray and Horne (21), Li (22) and Ohr (23) in Fe, Rohde and Pitt (24) and Feltham and co-workers (25) in Ni and Krausz (26) in ice.

The rate theory of stress relaxation (10)

In the rate theory, the stress dependence of the dislocation velocity has been shown to be

$$v(\tau_{eff}) = \nu \ell_f \exp\left(-(\Delta E_f^{\neq} - V_f \tau_{eff})/kT\right)$$

$$- \nu \ell_b \exp\left(-(\Delta E_b^{\neq} + V_b \tau_{eff})/kT\right)$$

The shear strain rate $\dot{\gamma}$ along the slip plane can be described by substituting the above expression in Orowan's equation

$$\dot{\gamma} = a\, b\, \rho_m\, v(\tau_{eff})$$

The tensile strain ϵ along the axis of loading is $\epsilon = C\gamma$ for a polycrystalline metal where C is a proportionality constant (27). Thus,

$$\dot{\epsilon}_p = C\, a\, b\, \nu\left[\rho_{m_f} \ell_f \exp\left(-(\Delta E_f^{\neq} - V_f \tau_{eff})/kT\right)\right.$$

$$\left. - \rho_{m_b} \ell_b \exp\left(-(\Delta E_b^{\neq} + V_b \tau_{eff})/kT\right)\right]$$

The plastic strain ϵ_p during stress relaxation is directly proportional to the observed stress change. Thus $\epsilon_p = -\Delta\sigma / E'$. The plastic strain rate is $\dot{\epsilon}_p$ is therefore

$$\dot{\epsilon}_p = (\partial \epsilon_p / \partial t)_{T,\, Str}$$

$$= -\frac{1}{E'} (\partial \Delta\sigma / \partial t)_{T,\, Str}$$

Thus the stress rate is $(\partial \Delta\sigma/\partial t) = -E' \dot{\epsilon}_p$

$$= -CE' a\, b\, \nu\left[\rho_{m_f} \ell_f \exp\left(-(\Delta E_f^{\neq} - V_f \tau_{eff})/kT\right)\right.$$

$$\left. - \rho_{m_b} \ell_b \exp\left(-(\Delta E_b^{\neq} + V_b \tau_{eff})/kT\right)\right]$$

The effective stress τ_{eff} in the above expression is the resultant of the applied shear stress τ_a and the internal stress τ_i. During stress relaxation, τ_i is assumed to be constant because the structure of the material does not change during the process. Therefore, $\tau_{eff} = \tau_a - \tau_i$. It was shown that (27)

$$\sigma_{eff} = 2\,\tau_{eff}$$

Hence, $\tau_{eff} = (\sigma_a - \sigma_i)/2$

$$= (\sigma_o + \Delta\sigma - \sigma_i)/2$$

where σ_o is the initial applied tensile stress. The equation for the stress relaxation process can now be written as,

$$\frac{\partial \Delta\sigma}{\partial t} = -\,C\,E'\,a\,b\,\nu\,\left[\rho_{m_f}\,\ell_f\,\exp\left(-(\Delta E_f^{\neq} - \frac{V_f}{2}(\sigma_o - \sigma_i + \Delta\sigma))/kT\right)\right.$$

$$\left. - \rho_{m_b}\,\ell_b\,\exp\left(-(\Delta E_b^{\neq} + \frac{V_b}{2}(\sigma_o - \sigma_i + \Delta\sigma))/kT\right)\right]$$

$$= -\,A_f\,\exp\,n_f\Delta\sigma + A_b\,\exp(-n_b\Delta\sigma) \qquad (1.5)$$

where,

$$A_f = C\,E'\,a\,b\,\rho_{m_f}\,\nu\,\ell_f\,\exp\left(-(\Delta E_f^{\neq} - \frac{V_f}{2}(\sigma_o - \sigma_i))/kT\right)$$

$$A_b = C\,E'\,a\,b\,\rho_{m_b}\,\nu\,\ell_b\,\exp\left(-(\Delta E_b^{\neq} + \frac{V_b}{2}(\sigma_o - \sigma_i))/kT\right)$$

$$n_f = V_f/2kT, \qquad n_b = V_b/2kT.$$

EFFECTIVE STRESS

Plastic deformation is controlled by the effective shear stress τ_{eff} acting on the dislocations. The effective stress is the resultant of the applied shear stress τ_a and the internal stress τ_i brought about by the crystal imperfections,

$$\text{Thus} \quad \tau_{eff} = \tau_a - \tau_i \tag{1.6}$$

The determination of the effective stress is therefore of great importance and is one of the central problems in the study of plastic deformation. Over the last two decades considerable effort was made to develop methods for the determination of the effective stress. Some of these proposed methods were extremely complex and were generally unsatisfactory.

In the last few years experimental methods were developed (28) based on the simple concept (Eqn. 1.6) that if

$$\tau_a = \tau_i$$

no dislocation movement takes place. In experiments using this concept, the internal stress and thus the effective stress can then be measured directly. The analysis of these tests inevitably leads to a rate equation with, at least two terms. Thus

$$\dot{\gamma} = - A'_f \exp\left(\frac{V_f \tau_{eff}}{kT}\right) + A'_b \exp\left(\frac{- V_b \tau_{eff}}{kT}\right) \tag{1.7}$$

where,

$$A'_f = \alpha b \rho_{m_f} \nu \ell_f \exp\left(- \Delta E_f^{\neq}/kT\right)$$

and $$A'_b = \alpha b \rho_{m_b} \nu \ell_b \exp\left(- \Delta E_b^{\neq}/kT\right)$$

Krausz (29) has pointed out that it follows from Eqn. (1. 7)that the dislocation stops at a finite terminal effective stress τ^{t}_{eff} rather than at zero effective stress. When the plastic deformation rate is zero Eqn. (1. 7) becomes,

$$0 = - A'_f \exp \left(\frac{V_f \tau^{t}_{eff}}{kT} \right) + A'_b \exp \left(\frac{-V_b \tau^{t}_{eff}}{kT} \right)$$

and hence,

$$A'_f \exp \frac{V_f \tau^{t}_{eff}}{kT} = A'_b \exp \left(\frac{-V_b \tau^{t}_{eff}}{kT} \right)$$

therefore,

$$\tau^{t}_{eff} = \frac{kT}{V_f + V_b} \ln \frac{A'_b}{A'_f} \qquad (1.8)$$

It follows from Eqn. (1. 8) that the proposed method cannot measure the effective stress when $A'_b \neq A'_f$. Because usually $A'_f < A'_b$ these methods underestimate τ_{eff}. When Eqn. (1. 7)can be integrated in closed form, then the effective stress can be calculated from the measured terminal applied stress. Krausz (29) has suggested that using this theory, the effective stress can be determined experimentally.

MacEwen and Ramaswami (28) proposed that by a combination of stress relaxation and strain relaxation, the value of the effective stress can be bracketed. Their method consists of first decreasing the applied stress by finite amounts until no further stress relaxation is observed (Fig. 1. 10). In the second stage of the measurements, the applied stress is instantaneously decreased below the internal stress level. The dislocations now experience an effective stress in the reverse direction $\tau_{eff} = \tau_a - \tau_i$ with $\tau_i > \tau_a$. If the specimen was loaded in tension, the large instantaneous stress-decrease causes contraction. After this contraction and with a stationary cross head, strain relaxation occurs by the same process as

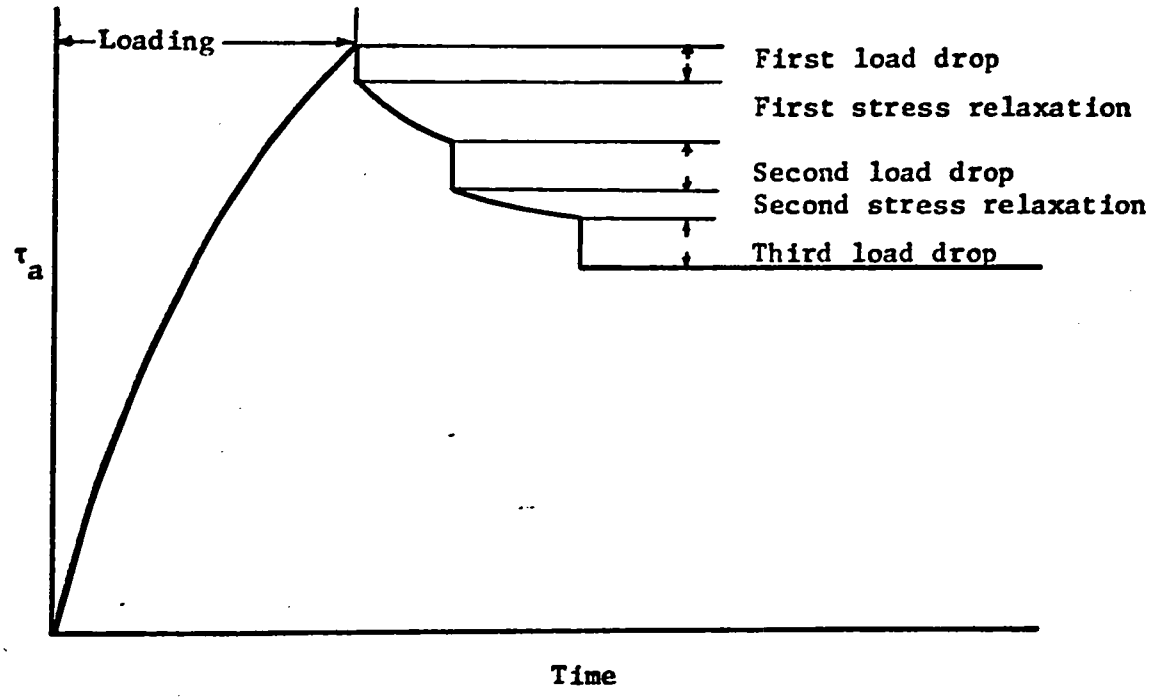

Fig. 1.10 The diagram shows the determination of effective stress using the stress relaxation method.

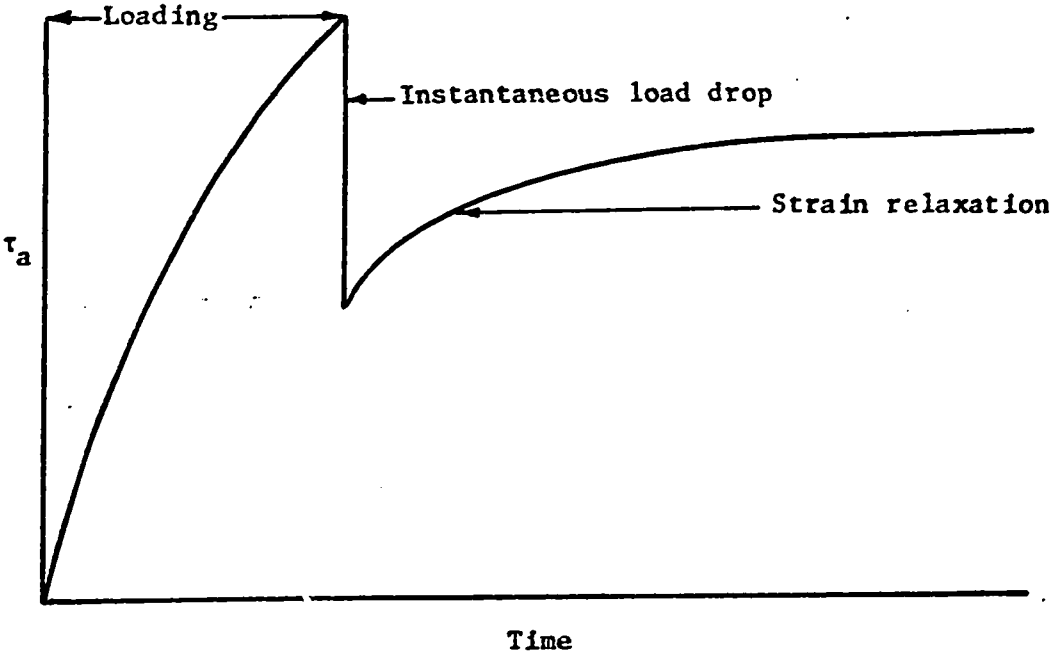

Fig. 1.11 The diagram illustrates the strain relaxation process.

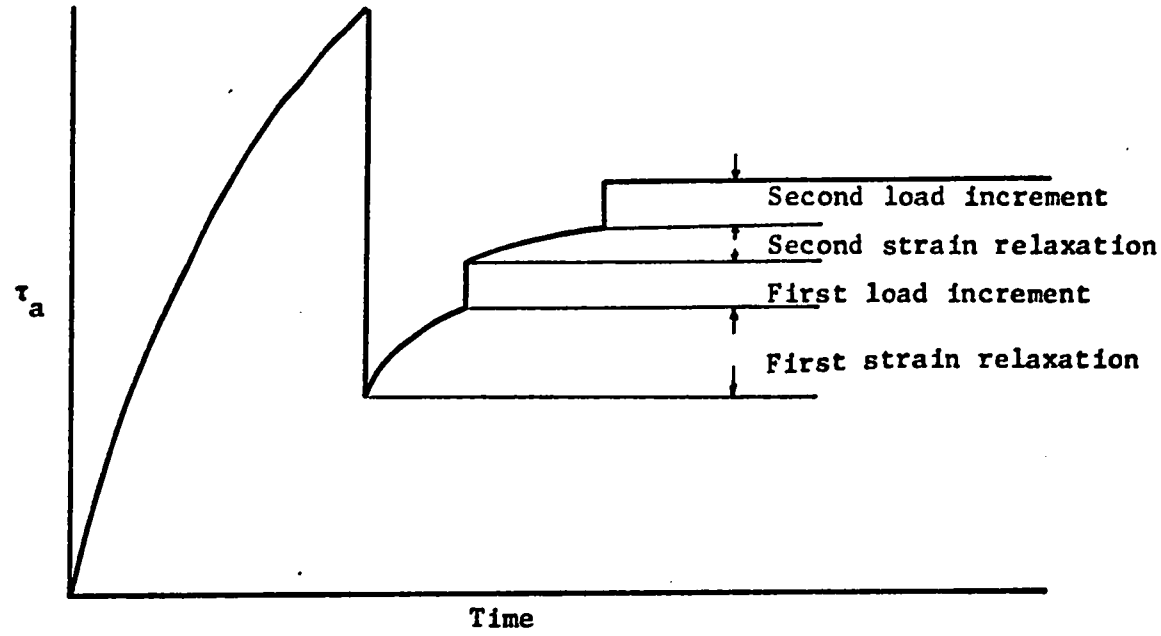

Fig. 1.12 The diagram indicates the determination of the effective stress using the strain relaxation method.

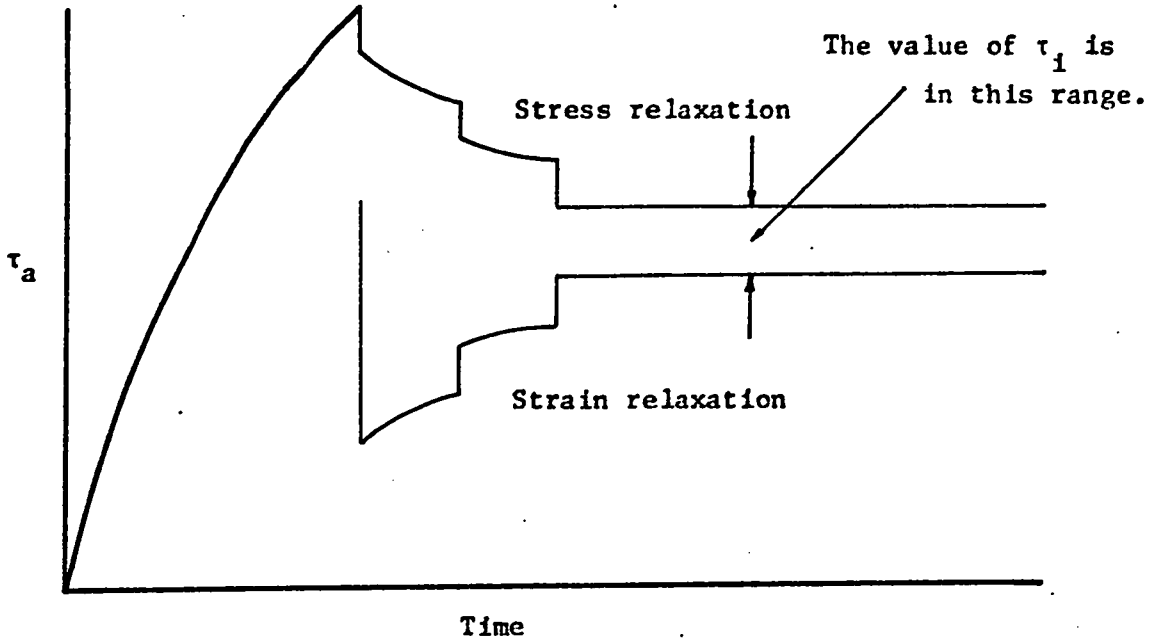

Fig. 1.13 The figure illustrates the determination of effective stress by the combination of stress and strain relaxation methods.

in stress relaxation but in the reverse direction. In consequence, the load increases in function of time as shown in Fig. (1. 11). Again, as in stress relaxation, if the load is increased by discrete amounts, strain relaxation can be stopped (Fig. 1. 12).

The combination of the above two tests brackets the value of the internal stress (Fig. 1. 13). The experiments carried out by MacEwen and Ramaswami substantiated the theoretical argument of Krausz that the value of τ_i cannot be measured but only a range can be established for τ_i . This type of experiment is nevertheless valuable because it indicates the approximate value of τ_{eff} for which almost no dependable information is available as yet.

2. EXPERIMENTAL PROCEDURE AND RESULTS

SPECIMEN PREPARATION

Specification and manufacture of the sintered iron powder compact

Supplier: Domtar Chemicals Ltd., Montreal.

Type : M. P. 32 Iron Powder.

Chemical Analysis:

ELEMENT	CONTENT %
C	0.02
S	0.02
P	0.02
Mn	0.15
Si	0.13
Acid Insolubles	0.23
F_e	Balance

Physical Properties:

Apparent Density = 2.45 g/cm^3.

Sieve Analysis:

- 80 + 100 = 1%
- 100 + 150 = 15%
- 150 + 200 = 27%
- 200 + 325 = 31%
- 325 = 26%

Preparation of the compacts:

The iron powder was blended with 1% Zinc Stearate - a compacting lubricant - for 30 minutes. Bars were pressed in a double acting die set at a compacting pressure of 5,000 Kg/cm^2 to a green density of 6.8 g/cm^3.

Sintering:

The green bars were presintered for six minutes at 650°C in Endogas to drive off the lubricant. They were cooled to room temperature and then sintered for 30 minutes at 1120°C in Endogas. (Endogas is a mixture of 40% H_2, 40% N_2 and 20% CO).

Typical properties of the above sintered compact:

Ultimate Tensile Strength 2100 Kg/cm^2

Impact (Unnotched Charpy) Strength 123 Kg cm.

Tensile Elongation (cm/cm) 5 - 10%

Machining

The specimens were machined from the above sintered compacts. The diameter of the machined specimen was 5.08 mm $\pm$ .025 mm and the effective length between the grips was 50.8 mm $\pm$ .13 mm (Fig. 2.1)

TESTING PROCEDURE

Stress Relaxation Tests

The preliminary tests were carried out on a Hounsfield Tensometer. The experimental arrangement of the Hounsfield Tensometer is shown in Fig. 2.2a. The tensometer was modified to increase the accuracy of the load read out. The core of a Linear Voltage Differential Transformer was mounted on the spring beam to measure the deflection of the beam. The voltage output of the transformer was recorded in function of time. To maintain the temperature of the system at 30.5 $\pm$ 0.75°C, an environmental chamber was built. The 0.75°C fluctuation caused a change in the stress of about 0.45 kg/cm^2 during stress relaxation.

The final tests were carried out on an Instron machine. A

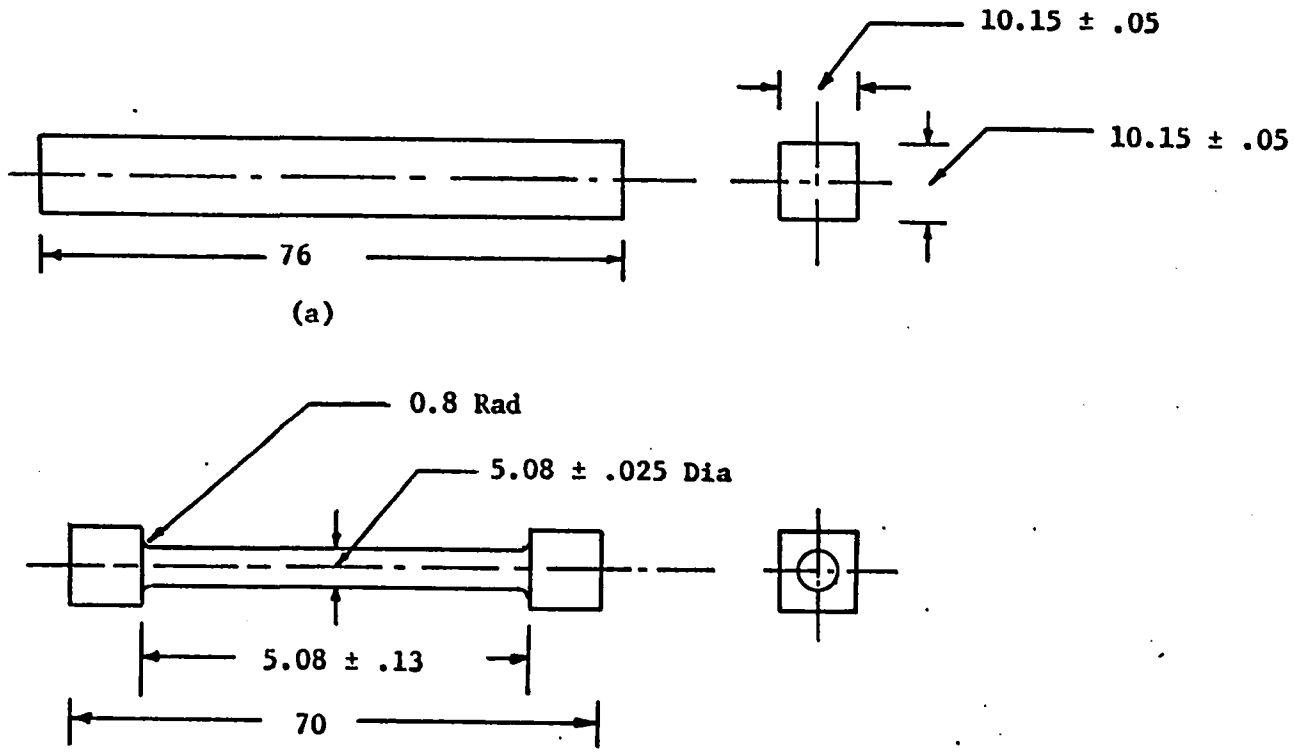

(a) As received compact

(b) Machined specimen

Fig. 2.1 The diagram shows the specimen used in the study.

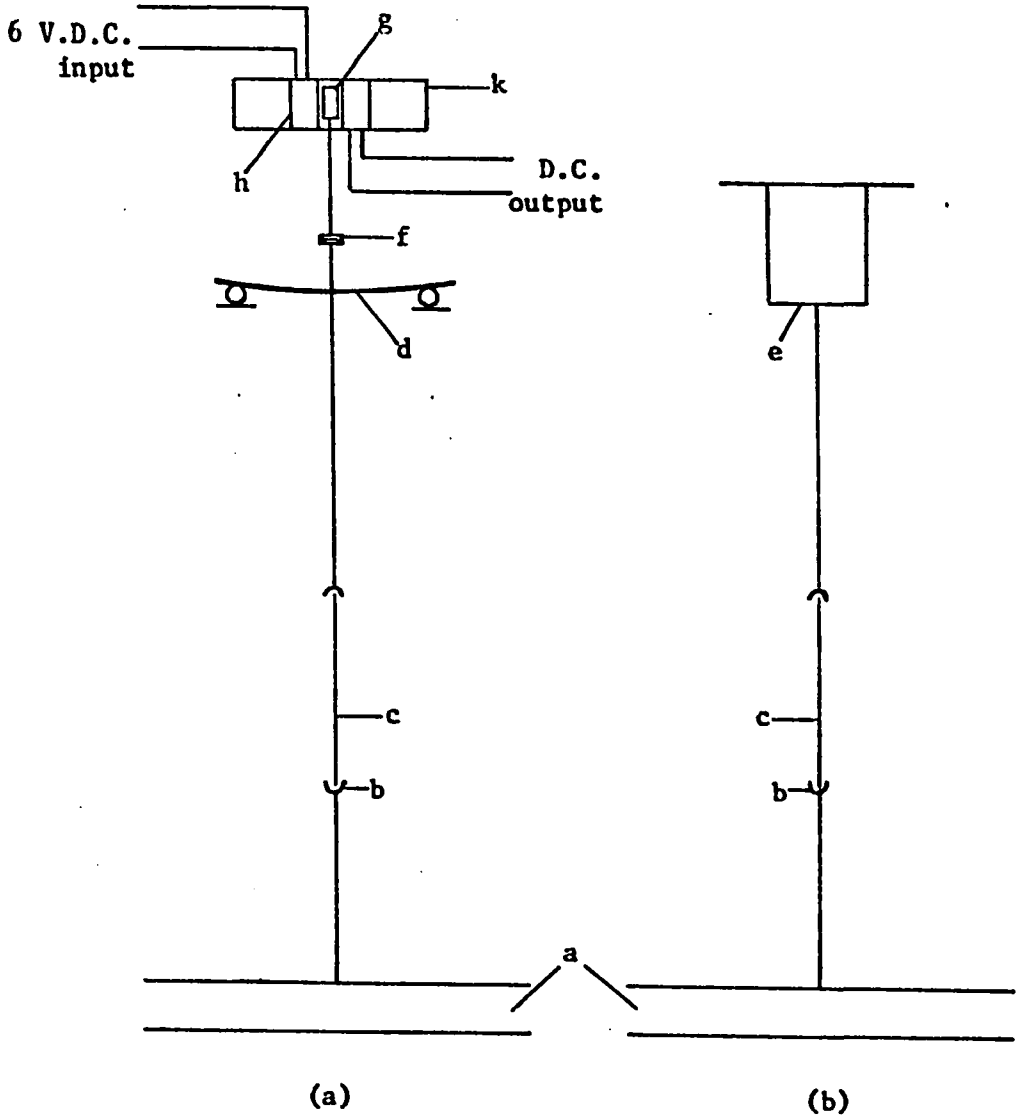

a. Cross head
b. Grips
c. Specimen
d. Spring beam
e. Load cell
f. Nuts for positioning the core
g. Core
h. Microformer
k. Microformer housing

Fig. 2.2 The figures show the experimental set up of a) the Hounsfield Tensometer and b) the Instron machine.

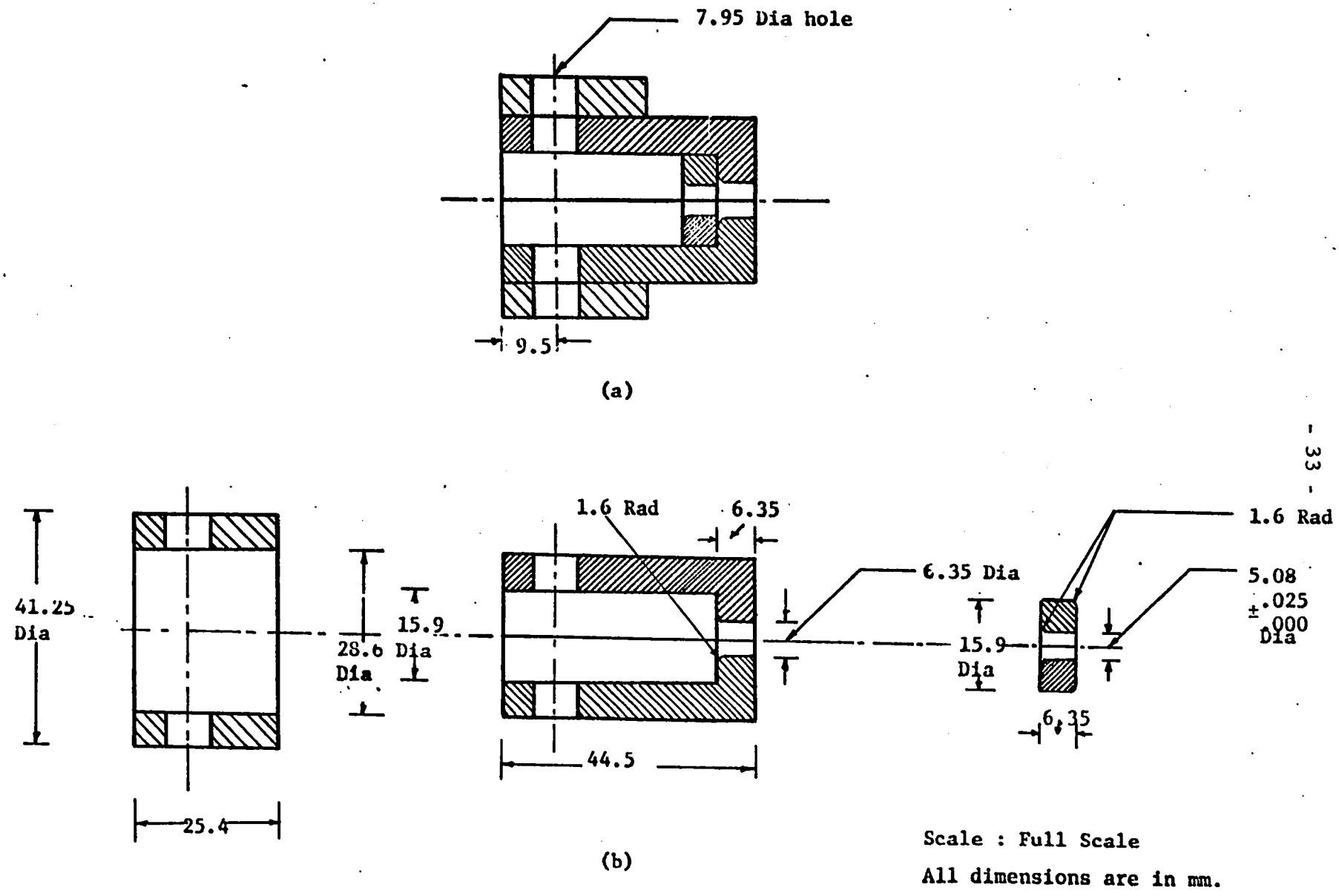

Fig. 2.3 The diagram shows the grips used to hold the specimen in the stress relaxation tests.
a) Assembled view
b) Details of parts

straingage type load cell of 1000 lb capacity was used to measure the load. A set of grips were designed to hold the specimen and to allign the load with the specimen axis. Fig. 2.3 shows the grips. The experimental set up on the Instron is shown in Fig. 2.2b. The specimen was held in the grips and after the temperature of the system stabilized, it was loaded at a uniform rate of 0.5 cm/min. After a predetermined stress level was reached, the cross head was stopped and was kept stationary. The decrease in load was recorded as a function of time. The tests were carried out for a period of time over which the temperature of the system remained within $\pm$ 0.5° C. Several tests were carried out on the same specimen at different stress levels till fracture occured. Table 2.1 gives the test conditions.

Internal Stress Measurements

Experiments were carried out to obtain information on the effective stress in sintered iron. The method utilized the theory of stress and strain relaxation (28), and was described in the introduction. 4 specimens were tested at various stress levels. The results are shown in Table 2.2.

Tensile Tests

Tensile tests were carried out on the sintered iron powder compacts at various strain rates to determine the effect of strain rate on the stress-strain characteristics. The applied load on the specimen was measured by the load cell. The elongation of the specimen was measured with a Linear Voltage Differential Transformer mounted on the grips. The outputs from the L. V. D. T. and the load cell were connected to an x-y recorder and the load-elongation relationship was plotted. Table 2.3 gives the test results.

TABLE 2.1

STRESS RELAXATION TEST CONDITIONS

SPECIMEN NUMBER	TEST NUMBER	STRESS LEVEL (kg/cm^2)	MACHINE USED
3	3.2	1530	Hounsfield
	3.3	1700	"
	3.4	1870	"
4	4.2	1530	"
	4.3	1700	"
5	5.1	1530	"
	5.2	1700	"
	5.3	1870	"
6	6.1	1530	"
	6.2	1700	"
	6.3	1870	"
7	7.1	1530	"
8	8.1	1593	Instron
	8.2	1700	"
	8.3	1890	"
9	9.1	1745	"
	9.2	1885	"
10	10.2	1885	"
11	11.1	1600	"
	11.2	1730	"
12	12.3	1705	"
	12.4	1890	"
13	13.1	1600	"
14	14.2	1703	"
	14.3	1890	"
15	15.1	1660	"

(Table 2. 1 continued)

SPECIMEN NUMBER	TEST NUMBER	STRESS LEVEL (kg/cm^2)	MACHINE USED
16	16.1	1615	Instron
	16.2	1710	"
	16.3	1895	"
17	17.1	1625	"
	17.2	1675	"
	17.3	1860	"
18	18.1	1633	"
	18.2	1690	"
	18.3	1910	"
19	19.1	1635	"
	19.2	1700	"
	19.3	1920	"

TABLE 2.2

INTERNAL STRESS DETERMINATION

TEST NUMBER	STRESS LEVEL (kg/cm^2)	INTERNAL STRESS (kg/cm^2)	
		Lower limit	Upper limit
16.2	1710	1440	1485
16.3	1895	1650	1780
17.3	1860	1610	1720
18.1	1633	1270	1450
18.2	1690	1310	1500
18.3	1910	1740	1790
19.1	1635	1405	1500
19.2	1700	1460	1520
19.3	1920	1675	1790
19.5	2000	1740	1850
20.1	1770	1560	1655
20.2	1815	1595	1690
20.3	1920	1720	1810
20.4	1975	1755	1870
20.5	2080	1860	1935

TABLE 2.3

TENSILE TEST RESULTS

TEST NO.	CROSSHEAD SPEED (cm /min)	YIELD STRENGTH (kg/cm^2)	ULTIMATE STRENGTH (kg/cm^2)	PERCENT ELONGATION IN 5 cm LENGTH
1	5.0	1350	2200	3.0
2	0.5	1700	2200	3.4
3	0.5	1500	2175	2.4
4	0.5	1750	2300	4.0
5	0.2	1650	2075	2.4
6	0.05	1500	2125	3.1
7	0.05	1650	2250	4.0
8	0.005	1250	2050	1.7

3. DISCUSSION

STRESS RELAXATION TESTS

The results of the stress relaxation tests are shown in Figs. 3.1 to 3.6 and 3.11. To facilitate the analysis, the tests are divided into 4 groups according to the initial stress level at which the stress relaxation was carried out. The groups are shown in Table 3.1.

TABLE 3.1

THE GROUPING OF THE STRESS RELAXATION TESTS

GROUP NUMBER	STRESS LEVEL kg/cm^2	TEST NUMBER
1	1615 $\pm$ 20	8.1, 11.1, 13.1, 16.1, 17.1, 18.1, 19.1
2	1700 $\pm$ 45	8.2, 9.1, 11.2, 12.3, 14.2, 15.1, 16.2, 17.2, 18.2, 19.2
3	1700 $\pm$ 30	11.2, 14.2, 17.2, 18.2, 19.2
4	1890 $\pm$ 30	8.3, 9.2, 10.2, 12.4, 14.3, 16.3, 17.3, 18.3, 19.3

From among the group 2 tests, 5 of the tests showed similar behaviour and they were grouped together to form group 3.

Figs. 3.1 to 3.4 show the logarithm of stress rate as a function of stress change. While the measured values are considerably scattered at the low stress levels, conspicuously less scatter was observed at the highest stress level. The probable reason for this behaviour is the following.

The structure, and therefore the plastic properties of the crystalline materials, is affected by the production method, heat treatment and the previous deformation history (30). At the low stress levels,

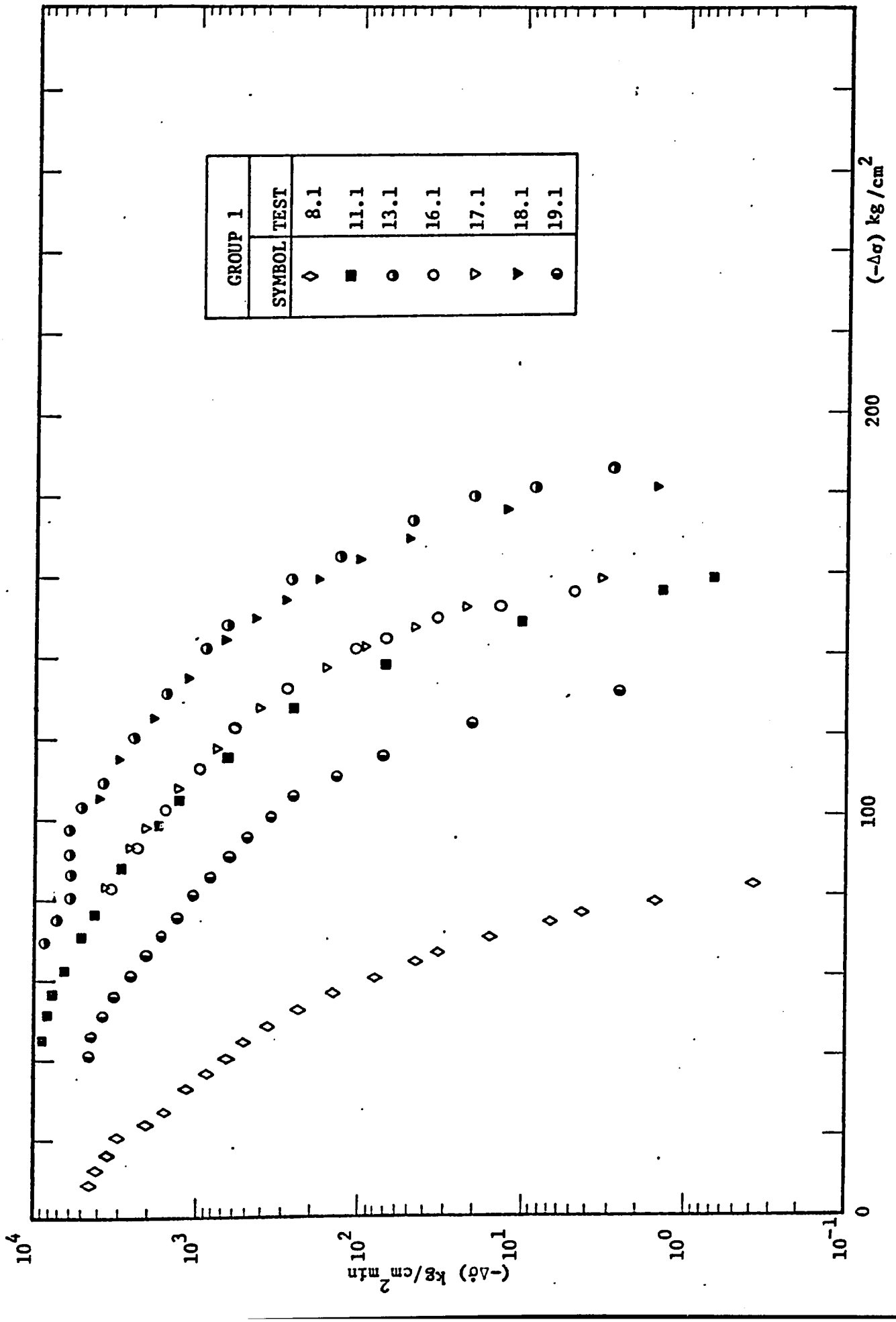

Fig. 3.1 The diagram illustrates the relation between $(-\Delta\sigma)$ and $\log(-\dot{\Delta\sigma})$ measured in the group 1 tests.

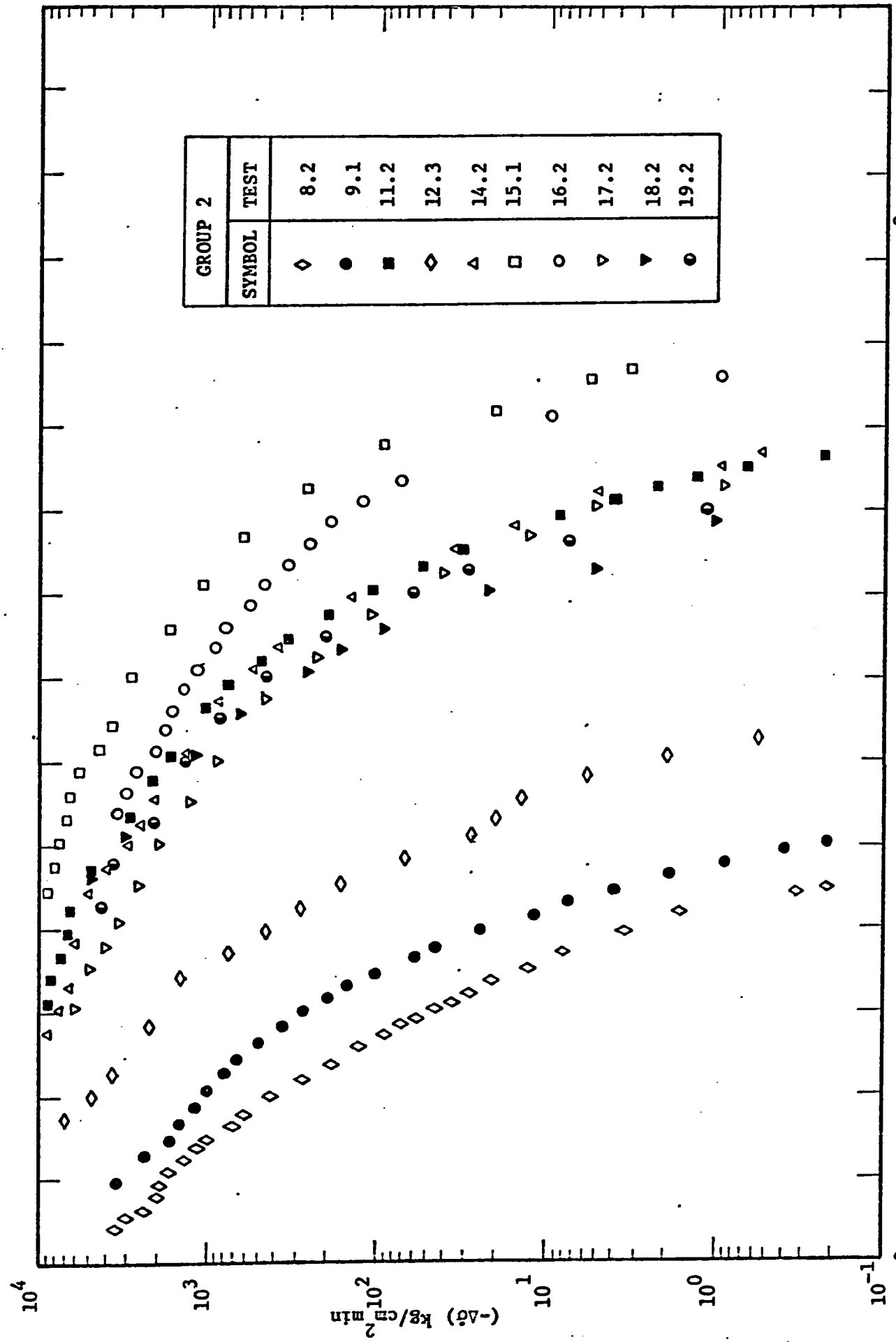

Fig. 3.2 The diagram illustrates the relation between $(-\Delta\sigma)$ and $\log(-\dot{\Delta\sigma})$ measured in the group 2 tests.

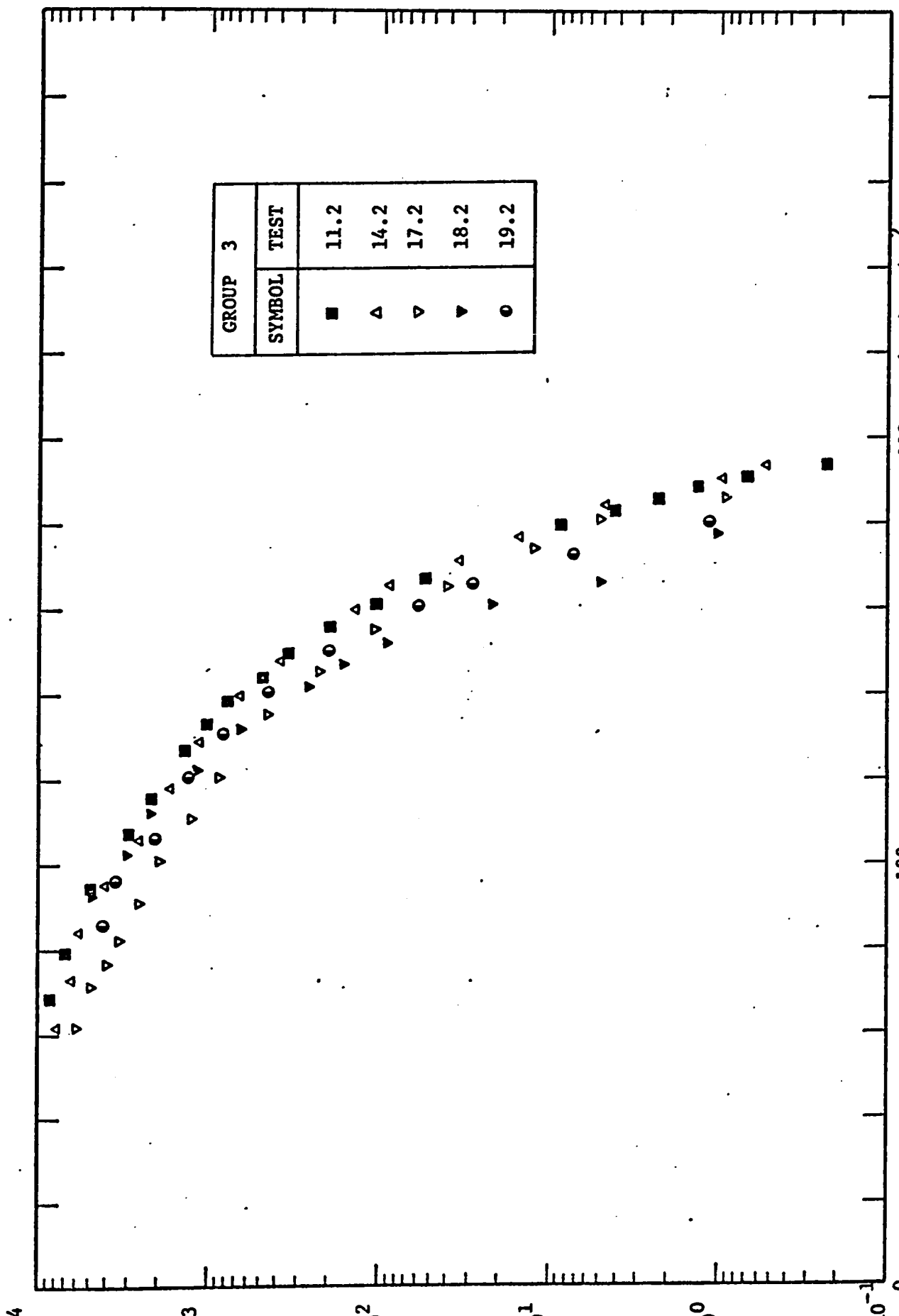

Fig. 3.3 The diagram illustrates the relation between $(-\Delta\sigma)$ and $\log(-\Delta\dot{\sigma})$ measured in the group 3 tests.

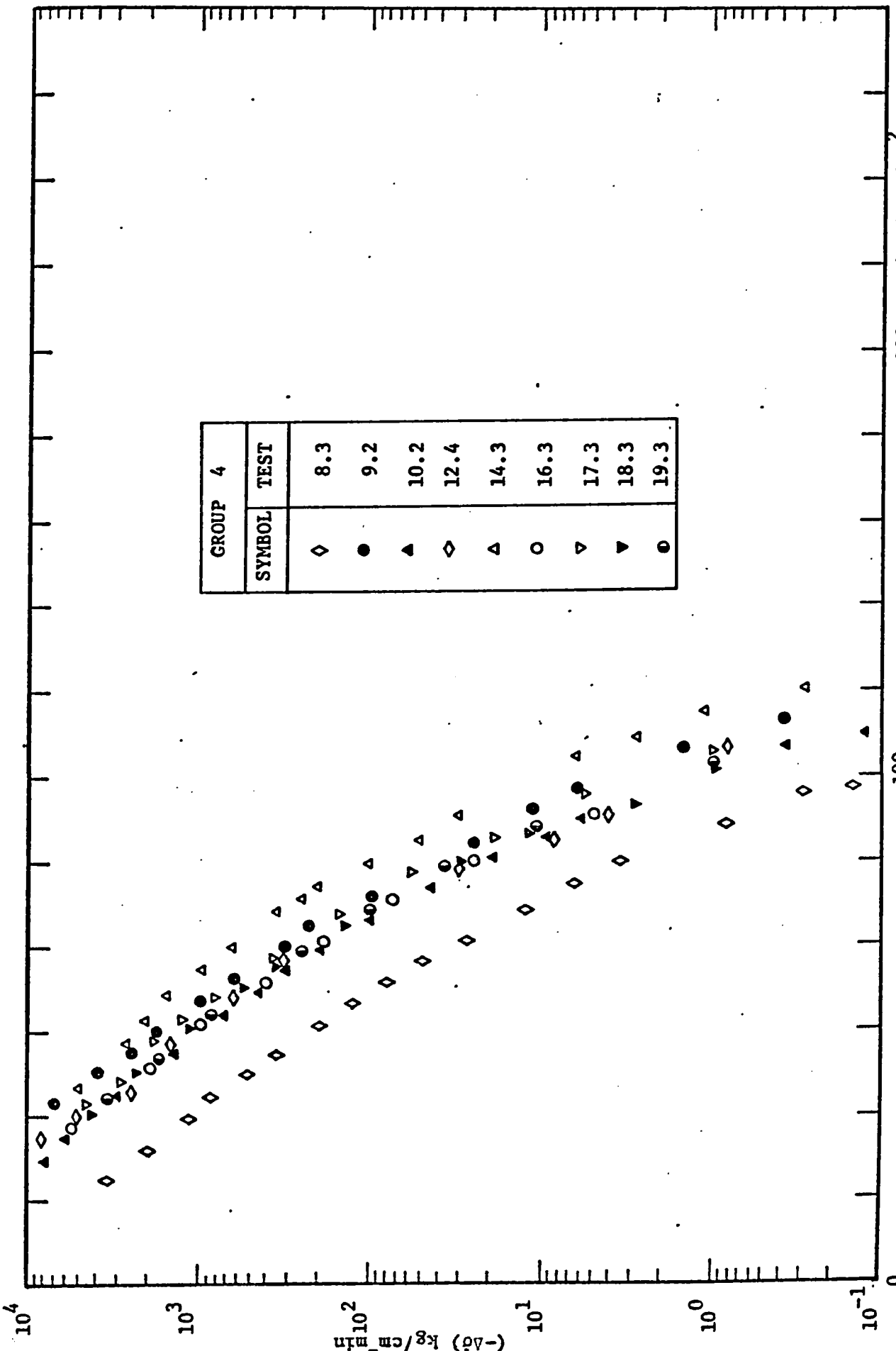

Fig. 3.4 The diagram illustrates the relation between $(-\Delta\sigma)$ and $\log(-\Delta\dot{\sigma})$ measured in the group 4 tests.

where the deformation is small, the effect of the production history is pronounced. Consequently, the difference in the structure of the material from one specimen to the other has a significant effect causing the observed scatter at the low stress levels. When, however, the stress level is high the deformation of the specimen is large and a new structure is developed which masks the pre-testing history. Therefore, the structure of the specimens are similar at the high stress level and the stress relaxation tests at this level give less scatter as illustrated in Fig. 3.4. The selection of group 3 specimens from group 2 indicates the transition zone from the scattered structure to uniform structure.

The stress change as a function of the logarithm of time is represented in Figs. 3.5 and 3.6 for the group 3 and group 4 tests respectively. The figures illustrate that the process slows down considerably after about 100 minutes.

The results of the group 3 and 4 tests were analyzed from Figs. 3.3 and 3.4 to determine the various parameters in the rate equation.

THE RATE THEORY ANALYSIS OF THE STRESS RELAXATION OF SINTERED IRON.

In the past almost all of the stress relaxation experiments have been carried out in the range where the log ($-\Delta\dot{\sigma}$) vs ($-\Delta\sigma$) relation is linear. Thus the analysis could be carried out with a one term expression

$$\Delta\dot{\sigma} = - A_f \exp(n_f \Delta\sigma)$$

neglecting the weaker, backward, activation process. In a few studies (22, 29, 31) tests were carried out over a long period of time and it was found that the relation log ($-\Delta\dot{\sigma}$) vs ($-\Delta\sigma$) deviates from linearity at the higher values of $|\Delta\sigma|$. This was explained by taking into consideration the effect of the backward movement of the dislocations. This effect is weak in the early, high stress, region and cannot be detected

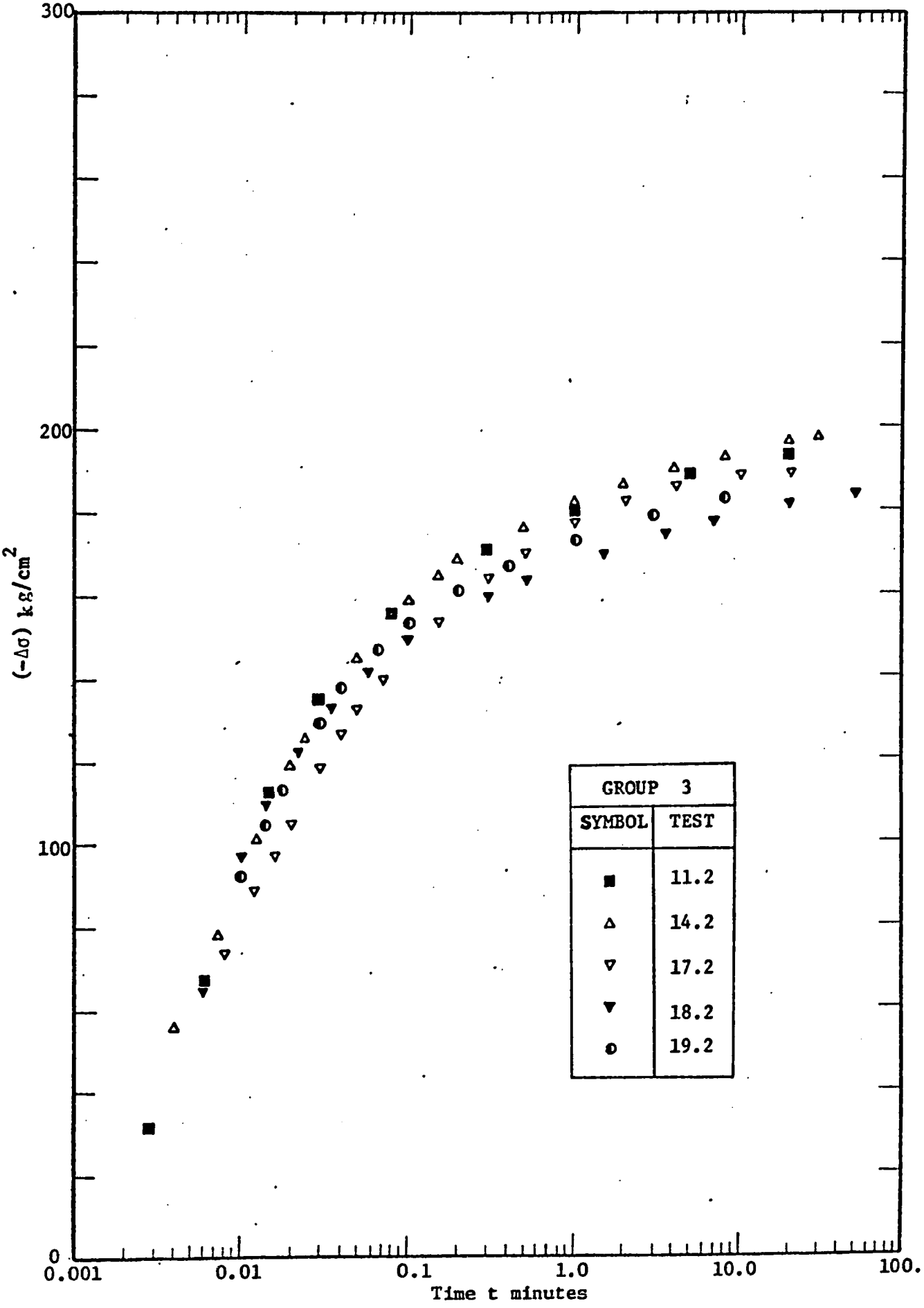

Fig. 3.5 The figure shows (-Δσ) in function of log t for group 3 tests.

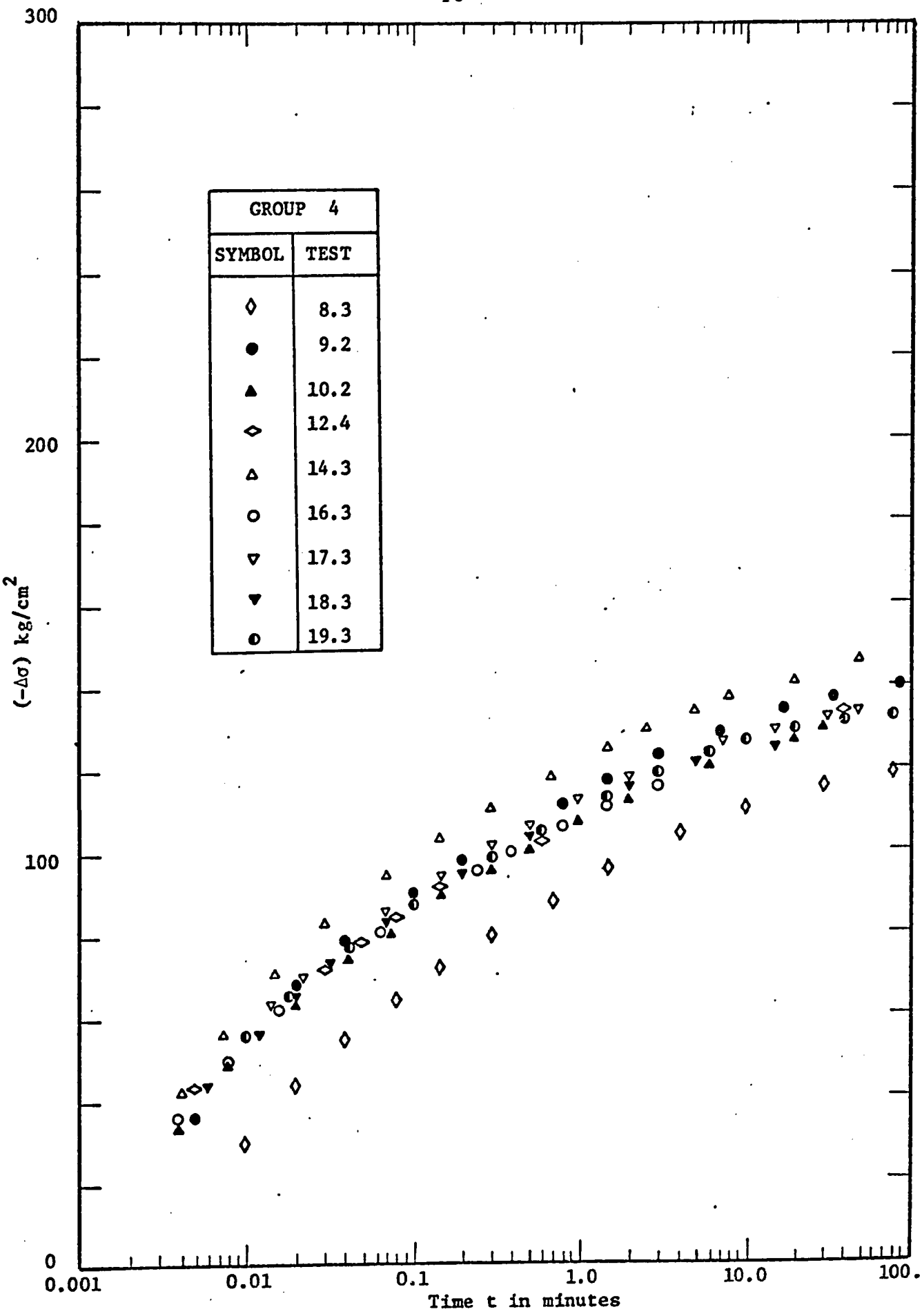

Fig. 3.6 The figure shows (-Δσ) in function of log t for group 4 tests.

within the sensitivity of the usual experimental systems. As the effective stress τ_{eff} decreases with increasing $|\Delta\sigma|$, the effect of the backward movement of the dislocations becomes noticeable and the rate equation is represented by two terms.

$$\Delta\dot{\sigma} = - A_f \exp (n_f \Delta\sigma) + A_b \exp (- n_b \Delta\sigma)$$

Very few stress relaxation experiments were carried out over a period long enough to decrease the effective stress until $(-\Delta\dot{\sigma}) \approx 0$. In the present investigation, effort was made to continue the stress relaxation tests until $(-\Delta\dot{\sigma})$ was nearly zero. A few tests were carried out on the Hounsfield tensometer for a period of 3 days. The measured stress rate range covered as much as five orders of magnitude, the practically feasible full range of measurements. Any further significant extension is a highly complex experimental problem requiring extremely sensitive recording instruments and a very stable, temperature controlled environment. Furthermore, even if the sophisticated instrumentation is available, the duration of the test, to cover only one more order of magnitude, would be prohibitively long—about 30 to 40 days. Because the stress change over this additional decade is already very small, the information obtained could not add significantly to the data available from the present experiments. A meaningful extension would require several more orders of magnitude in the $\Delta\dot{\sigma}$ values to be measured, a series of tests each running over years.

The analysis of the results obtained over the full practically feasible, five orders of magnitude, range indicates that the two term rate equation is not sufficient any longer when $|\Delta\dot{\sigma}|$ is very small. In this range it is expected that a second rate controlling mechanism may become noticeable. Retaining the conditions which lead to the two term rate equation, the stress change in this region can be described by the

following expression (Fig. 3.7)

$$\Delta\dot{\sigma} = \left[- A_f \exp (n_f \Delta\sigma) + A_b \exp (-n_b \Delta\sigma)\right]_I$$

$$+ \left[- A_f \exp (n_f \Delta\sigma) + A_b \exp (-n_b \Delta\sigma)\right]_{II}$$

where the subscripts I and II indicate that the parameters A and n are associated with the first and second mechanisms respectively and may have different values.

The analysis is complex and tedious when more than one mechanism controls the deformation. When there are m independent (parallel) processes associated with the plastic deformation, the rate equation may be represented by

$$\Delta\dot{\sigma} = \sum_{i=1}^{m} \left[- A_f \exp (n_f \Delta\sigma) + A_b \exp (-n_b \Delta\sigma)\right]_i$$

When i = 1, the validity limit for the rate equation can be determined as follows.

Over the range where the first process is predominant,

$$\Delta\dot{\sigma} = - A_f \exp (n_f \Delta\sigma) + A_b \exp (-n_b \Delta\sigma) \qquad (3.1)$$

However, when $|\Delta\sigma|$ is small, the relation reduces to

$$\Delta\dot{\sigma} = - A_f \exp (n_f \Delta\sigma)$$

Hence $\ln (-\Delta\dot{\sigma}) = \ln A_f + n_f \Delta\sigma$

Thus the $\ln (-\Delta\dot{\sigma})$ vs $(-\Delta\sigma)$ relation is represented by a straight line with a slope of $-n_f$ and an intercept of $\ln A_f$ at $\Delta\sigma = o$. When

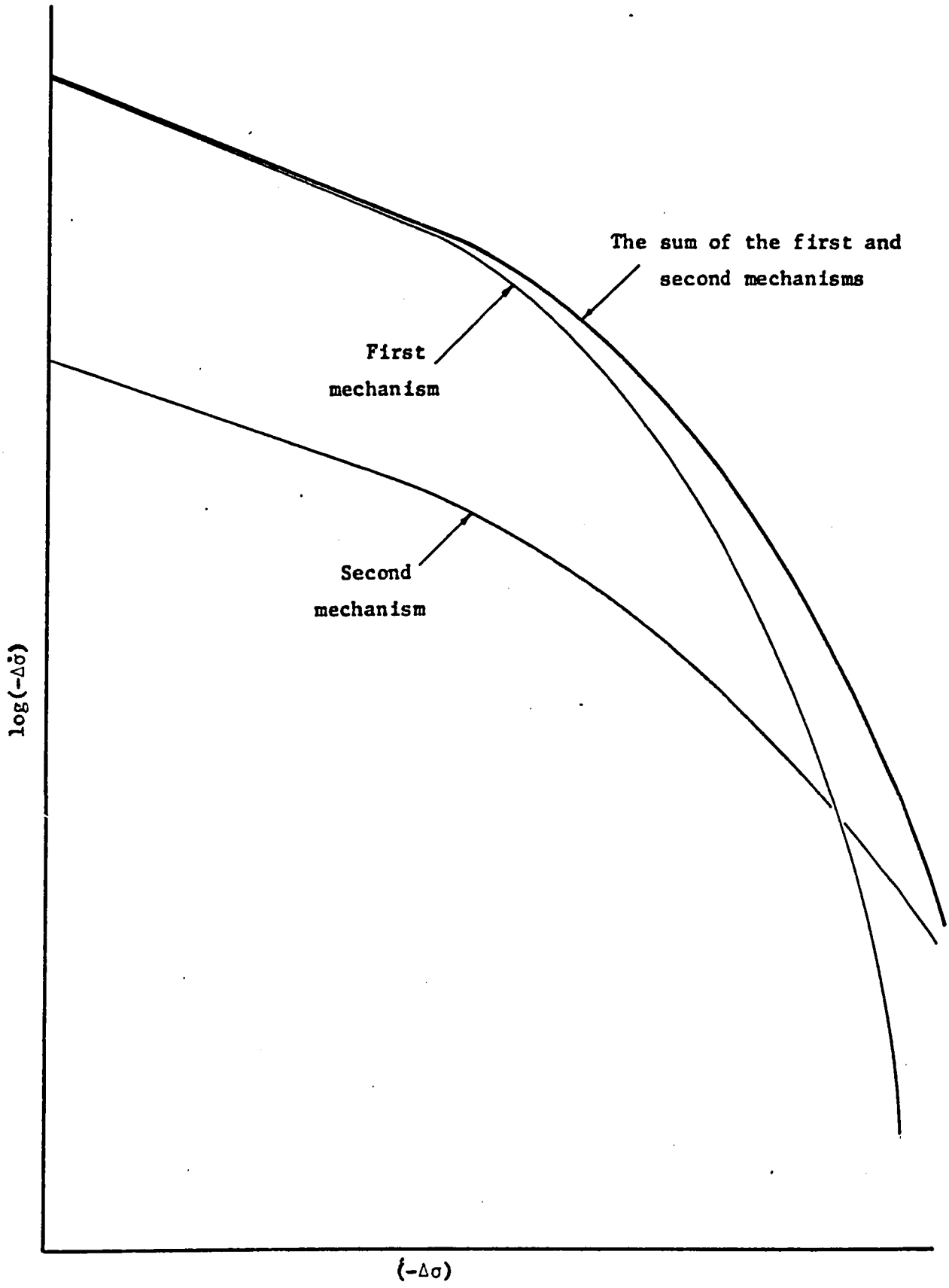

Fig. 3.7 The diagram illustrates the effect of a second mechanism on the stress relaxation process.

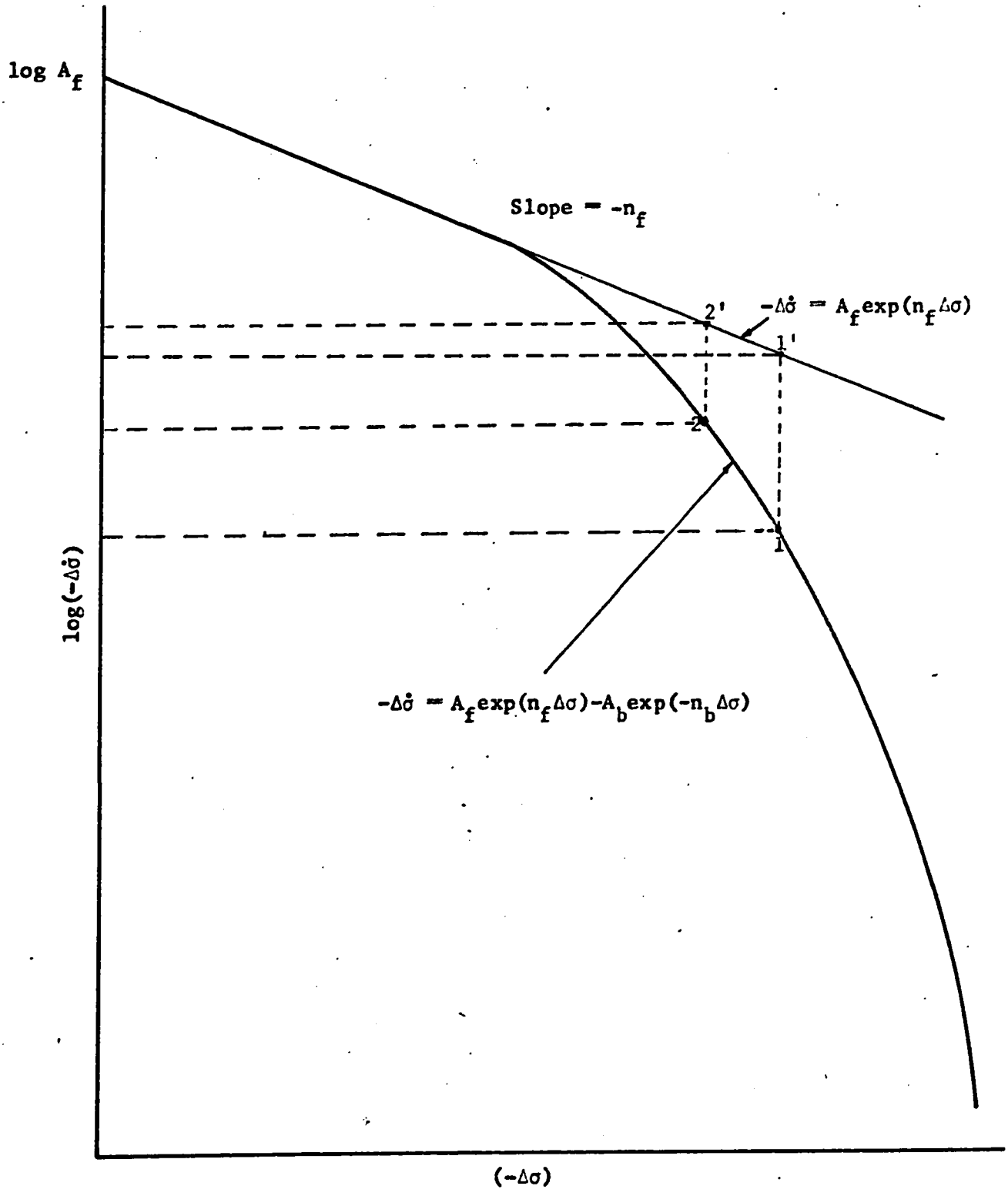

Fig. 3.8 The figure illustrates the determination of the validity limit for the two term rate equation.

$|-\Delta\sigma|$ is not small then, within the validity limit of the process i = 1, both terms have to be considered. The parameters A_f and n_f are determined from the linear portion of the $\ln(-\Delta\dot{\sigma})$ vs $(-\Delta\sigma)$ relation (small $|\Delta\sigma|$ range). For the second term, the analysis is carried out (Fig. 3.8) in the following manner. Consider two points 2 and 1 in the i = 1 zone, where 1 is at the validity limit of the two term expression. Using Eqn. (3.1) and solving for n_b and A_b we get,

$$n_b = \frac{1}{\Delta\sigma_2 - \Delta\sigma_1} \ln \frac{\Delta\dot{\sigma}_1 + A_f \exp(n_f \Delta\sigma_1)}{\Delta\dot{\sigma}_2 + A_f \exp(n_f \Delta\sigma_2)}$$

and $A_b = [A_f \exp(n_f \Delta\sigma_2) + \Delta\dot{\sigma}_2] \exp(n_b \Delta\sigma_2)$

These expressions are physically meaningful only if $n_b > o$, with $\Delta\sigma_2 - \Delta\sigma_1 > o$.

Referring now to Fig. 3.8 it follows that

$$(-\Delta\dot{\sigma}_{2'}) - (-\Delta\dot{\sigma}_2) = A_f \exp(n_f \Delta\sigma_2) - [(A_f \exp(n_f \Delta\sigma_2) - A_b \exp(-n_b \Delta\sigma_2)]$$

$$= A_b \exp(-n_b \Delta\sigma_2)$$

Similarly $(-\Delta\dot{\sigma}_{1'}) - (-\Delta\dot{\sigma}_1) = A_b \exp(-n_b \Delta\sigma_1)$.

It follows that n_b is positive if

$$A_b \exp(-n_b \Delta\sigma_1) > A_b \exp(-n_b \Delta\sigma_2)$$

Therefore

$$(-\Delta\dot{\sigma}_{2'}) - (-\Delta\dot{\sigma}_{2}) \leq (-\Delta\dot{\sigma}_{1'}) - (-\Delta\dot{\sigma}_{1})$$

This is the condition for the validity of the two term rate equation. Using this expression, an upper validity limit for the two term expression can be read off immediately from the graphical representation shown in Fig. 3.8.

The results of the group 3 and 4 tests were analyzed to determine A_f and n_f from the initial portion of the stress relaxation curve in Figs. 3.3 and 3.4 and are presented in Table 3.2.

TABLE 3.2

THE ACTIVATION PARAMETERS IN SINTERED IRON

GROUP	STRESS LEVEL kg/cm^2	A_f $kg/cm^2 min.$	n_f cm^2/kg	V_f $\mathring{A}^3$	b^{3*}
3	1700 ± 30	210,000	0.0411	3430	224
4	1890 ± 30	80,000	0.0677	5650	370

Stress relaxation results are usually analyzed within the framework of the conditions leading to Eqn. (1.5). The determination of the rate controlling mechanism is inevitably an extremely lengthy process and a complex problem.

The present investigation indicates that, because the activation volume is in the order of $10^2 b^3$, or less, plastic deformation in sintered iron may occur either by dislocation intersection mechanism or by the overcoming of energy barriers associated with the impurities. It has to be emphasized that the present study is only a first approximation in the analysis of the rate process. A full investigation requires a detailed metallographic examination and rate theory study.

The validity limit of the two term rate equation was determined in the group 3 and 4 tests. The results are shown in Table 3.3

* b for iron is 2.48×10^{-8} cm. (32)

TABLE 3.3

THE VALIDITY LIMIT OF THE TWO TERM RATE EQUATION

GROUP	STRESS LEVEL kg/cm^2	$-\Delta\sigma_1$ kg/cm^2	$-\Delta\dot{\sigma}_1$ kg/cm^2 min.	t_1 Min.
3	1700 ± 30	155	320	0.1
4	1890 ± 30	98	90	0.25

The above results indicate that the effect of the second rate controlling mechanism is significant after ~. 1 minutes when $|\Delta\dot{\sigma}|$ is less than ~ 320 kg/cm^2 min.

It is possible to identify tentatively the second rate controlling mechanism (33). In body centred cubic iron, the interstitial atoms are in the positions shown in Fig. 3.9 These atoms distort the lattice and increase the crystal energy. When the crystal is in a stress free condition, the x, y, z positions are energetically equivalent and the number of interstitial atoms moving out of any position is equal to those moving into it. A tensile stress applied along the z axis elongates the crystal in this direction and there is more space available in the z positions. The occupation of these now requires less energy. In consequence, there is a net flow of the interstitial atoms from the x and y into the z positions. This contributes an additional lattice distortion in the z direction. Hence, when a tensile stress is applied, there is a simultaneous elastic elongation as shown in Fig. 3.10, followed by the diffusion of the interstitial atoms into the energetically favourable sites causing a time dependent, thermally activated, additional deformation. This anelastic deformation approaches assymptotically to a finite limit as the equilibrium interstitial distribution, corresponding to the applied stress, is reached.

The strain associated with this process is expected to be in the

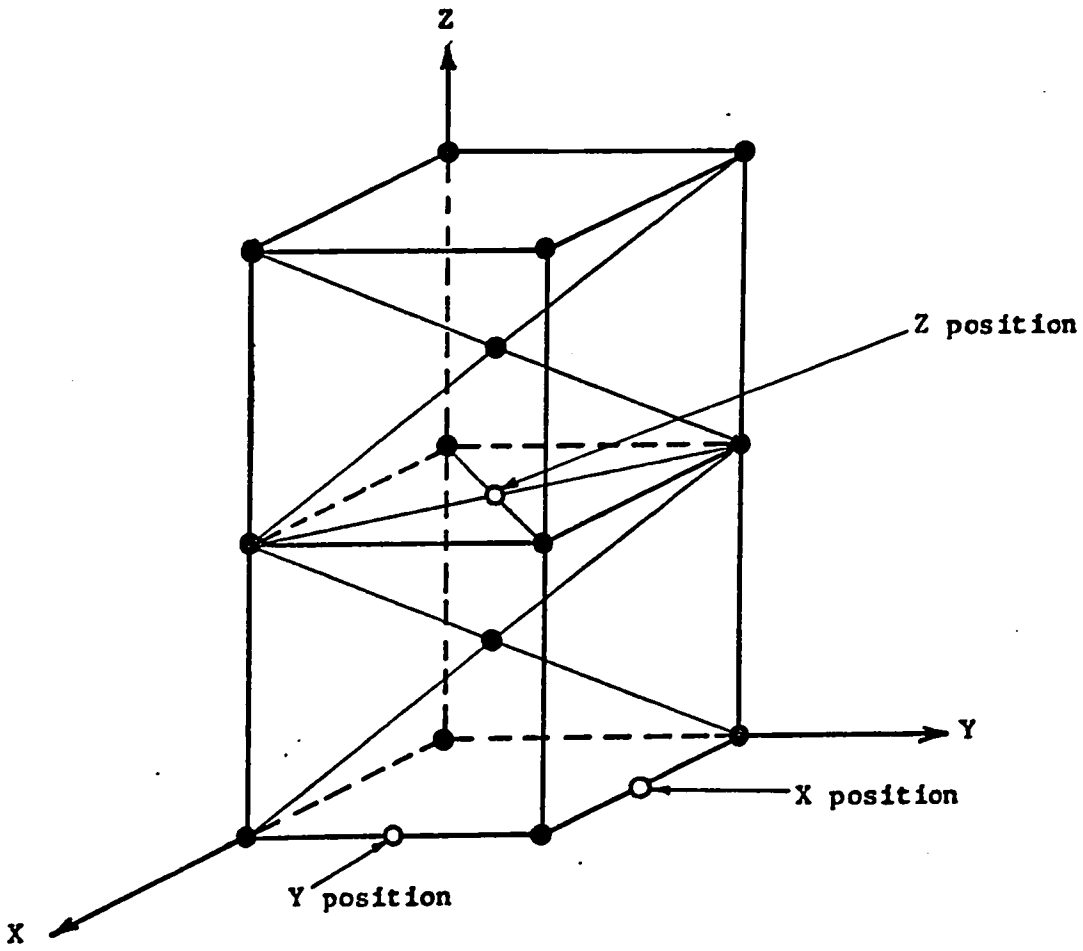

Fig. 3.9 The figure shows the iron atoms (●) and the interstitial atoms (o) in b.c.c. iron.

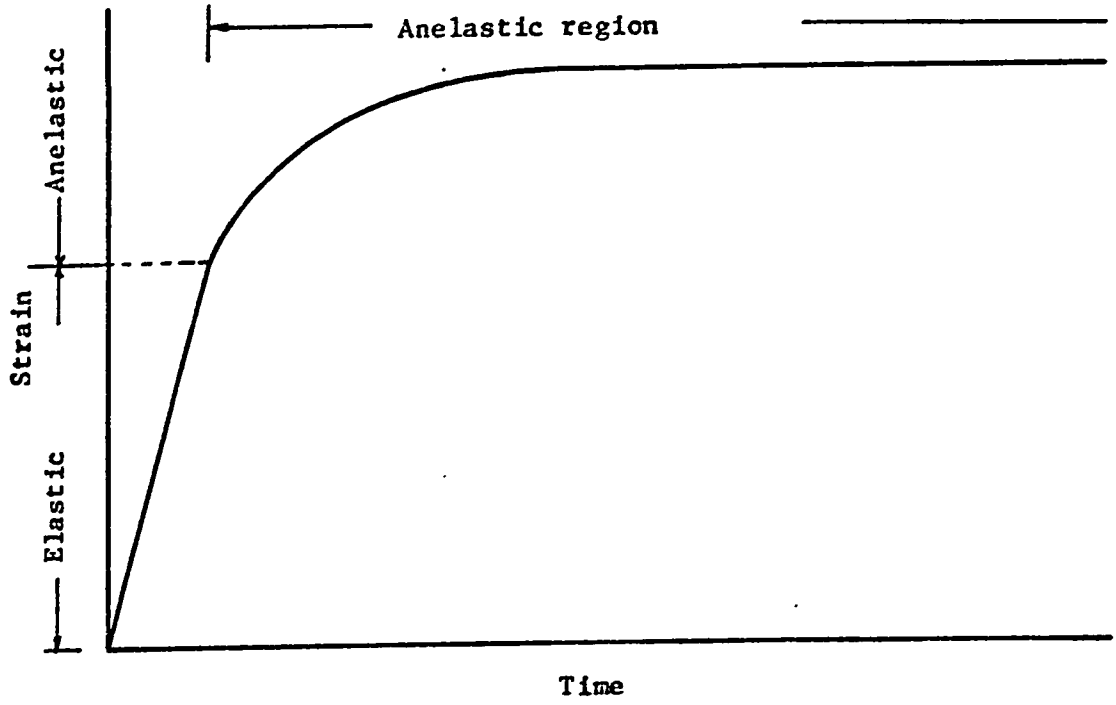

Fig. 3.10 The diagram illustrates the anelastic strain produced by the diffusion of the interstitial atoms in iron.

order of 10^{-5} and the effect is therefore not noticeable in the first two stages of stress relaxation. After the first two terms become very small, however, this additional strain is noticeable. Even though the process is slow at room temperature, compared to the dislocation movement, its effect was detected after ~ 0.1 minutes.

THE DETERMINATION OF THE STRESS EXPONENT m

The power function expression relating strain rate and stress and derived from the equation

$$v = v_o(\tau_a/\tau_o)^m \qquad (3.2)$$

is often used in the engineering studies of plastic deformation. It is of interest therefore to investigate the behaviour of sintered iron in terms of this equation. The results of the stress relaxation tests were analysed to determine the value m in Eqn. (3.2). The analysis was carried out as follows.

Substituting the expression for v in Orowan's equation

$$\dot{\gamma} = \alpha b \rho_m v$$

and using the relations $\epsilon = C\gamma$ and $\sigma = 2\tau$, the normal strain rate $\dot{\epsilon}$ is

$$\dot{\epsilon} = C \alpha b \rho_m v_o (\sigma_a/\sigma_o)^m$$

During stress relaxation,

$$\dot{\epsilon} = - \Delta\dot{\sigma} / E'$$

Hence
$$-\Delta\dot{\sigma} = E'\dot{\epsilon}$$
$$= E' C \alpha b \rho_m v_o(\sigma_a/\sigma_o)^m$$
$$= C_1 \sigma_a^m$$

where
$$C_1 = E' C \alpha b \rho_m v_o(1/\sigma_o)^m$$

Therefore, m can be determined from the slope of the plot of the log $(-\Delta\dot{\sigma})$ as a function of log σ_a as given in Fig. 3.11 for the group 3 and 4 tests.

In engineering tests it is customary to consider m to be constant. The analysis of the results represented in Fig.3.11 however, indicated that m was not a constant for sintered iron, but varied with the applied stress. Therefore, the curves in Fig. 3.11 were approximated by two straight lines and two values, m_1 and m_2, were determined from the slope of these lines. m_1 and m_2 are the slopes at the initial and later portions of the stress relaxation respectively(Fig. 3.11b). The results are given in Table 3.4.

TABLE 3.4

THE STRESS EXPONENT m IN SINTERED IRON

GROUP	STRESS LEVEL (kg/cm^2)	m_1	m_2
3	1700 ± 30	67	286
4	1890 ± 30	132	222

The slope m increases as the relaxation proceeds. Therefore m_1 overstimates the strain rate at the later portions of stress relaxation and m_2 underestimates the strain rate at the earlier portion of stress relaxation.

INTERNAL STRESS

The results of the internal stress measurement (Table 3.5) indicate that the internal stress in sintered iron is

$$\tau_i \approx (0.89 \pm .03)\ \tau_a$$

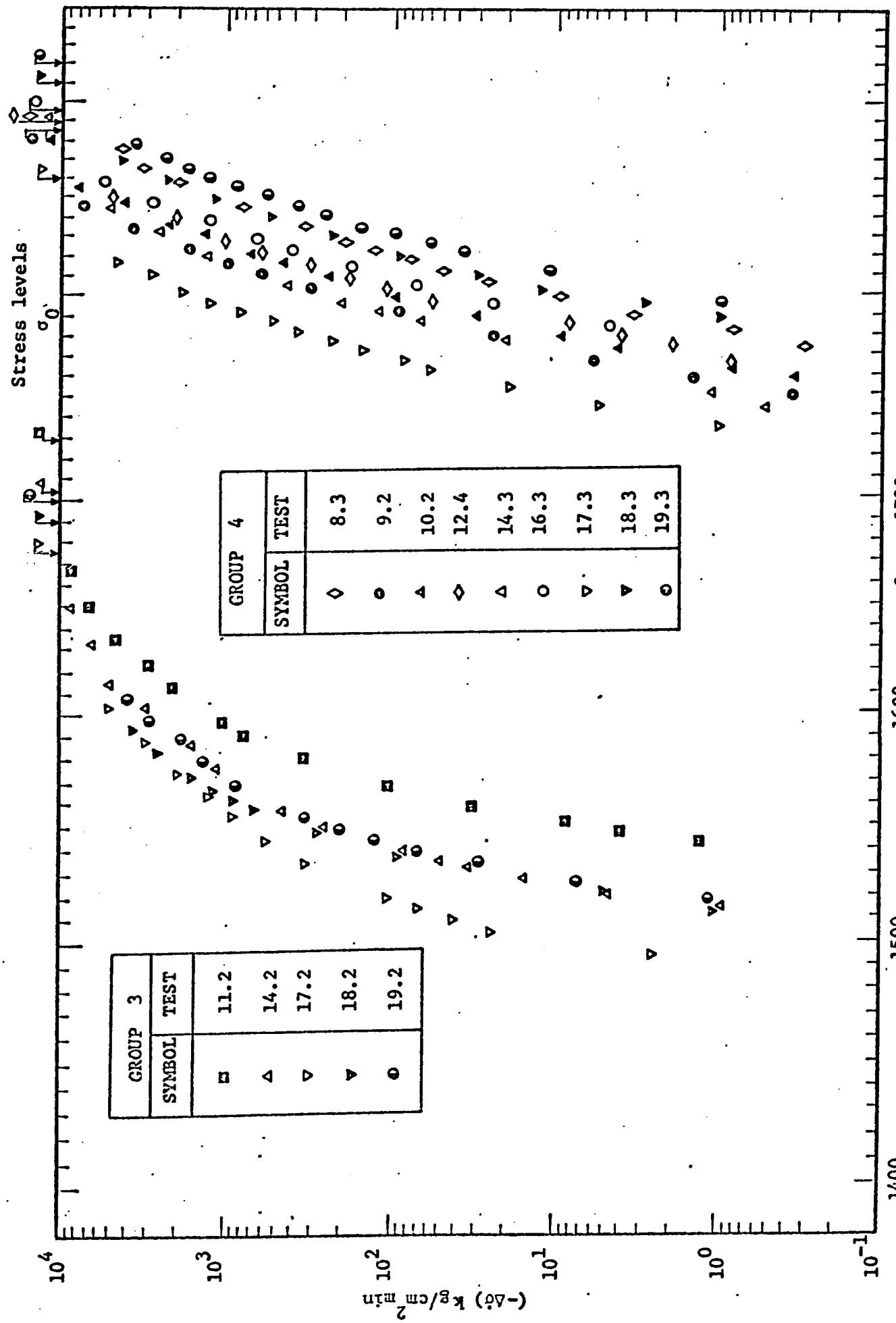

Fig. 3.11a The figure illustrates the dependence of $\log(-\Delta\dot{\sigma})$ on $\log \sigma_a$ for the group 3 and group 4 tests.

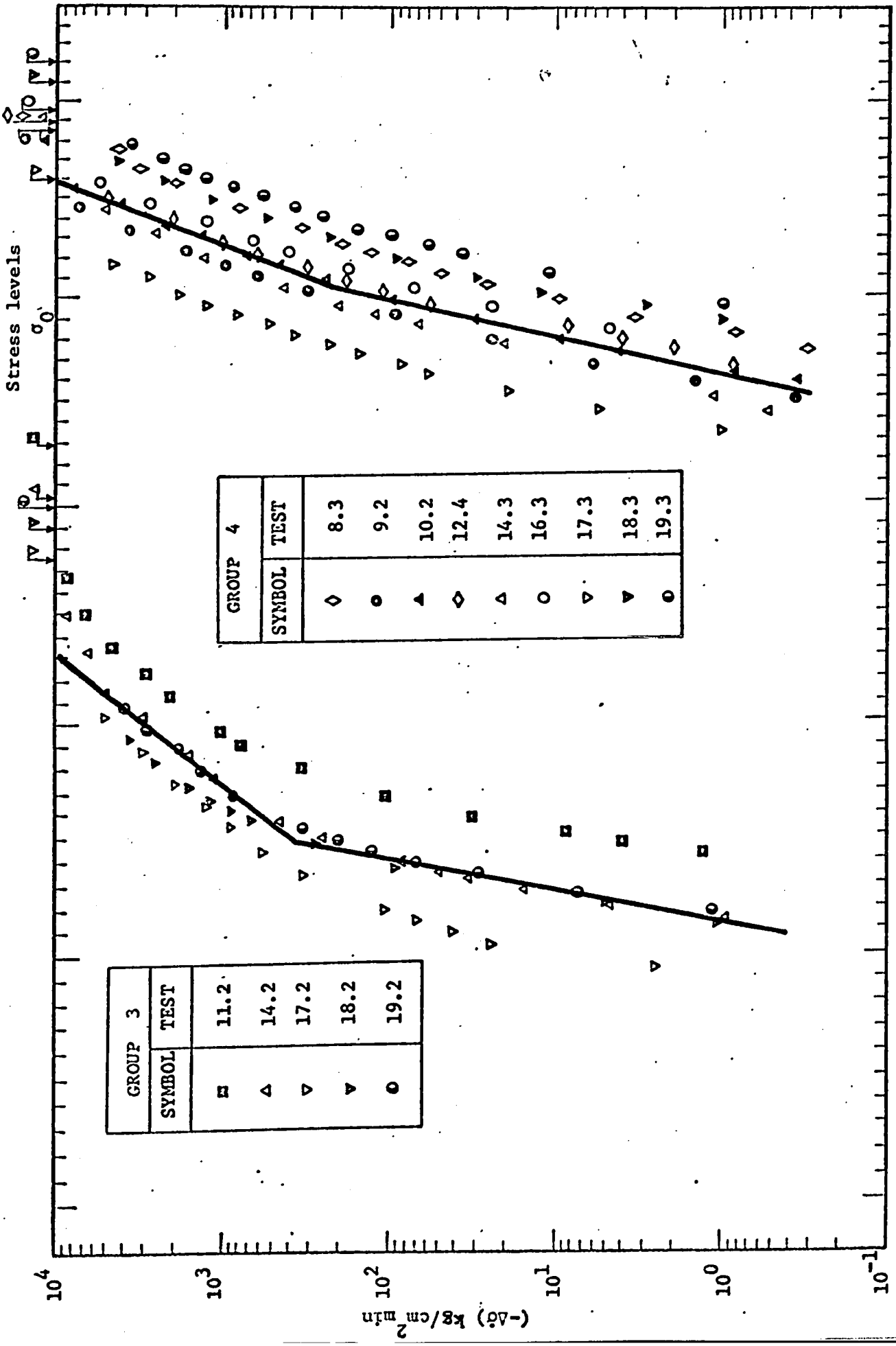

Fig. 3.11b The diagram illustrates the determination of the stress exponent m in sintered iron for the group 3 and group 4 tests.

This result is of interest because, as mentioned before, very little information is available on the effective stress in general. Furthermore, a knowledge of the approximate value of τ_{eff} is important in the analysis of the thermally activated dislocation movement, and in the interpretation of the plastic behaviour of sintered iron.

TABLE 3.5

THE INTERNAL STRESS IN SINTERED IRON

TEST NUMBER	STRESS LEVEL (kg/cm^2)	INTERNAL STRESS AS A PERCENTAGE OF THE STRESS LEVEL
16.2	1710	85 ± 2
16.3	1895	91 ± 4
17.3	1860	89.5 ± 3
18.1	1633	83 ± 6
18.2	1690	83.5 ± 6
18.3	1910	92 ± 2
19.1	1635	89 ± 3
19.2	1700	87.5 ± 2
19.3	1920	90 ± 3
19.5	2000	90 ± 3
20.1	1770	91 ± 3
20.2	1815	90 ± 3
20.3	1920	92 ± 3
20.4	1975	92 ± 3
20.5	2080	91 ± 2

TENSILE TESTS

Tensile tests were carried out on the sintered iron powder compacts at various strain rates. The specimens were identical to those used in the stress relaxation tests. The tensile test results are given in Table 3.6.

A change in the strain rate from 0.001/min to 1/min did not produce any consistent variation in the stress-strain characteristics.

TABLE 3.6

TENSILE TEST RESULTS IN SINTERED IRON

TEST NUMBER	STRAIN RATE (1/min)	SLOPE IN THE PRE-YIELD RANGE (kg/cm^2)
1	1.0	80×10^4
2	0.1	51×10^4
3	0.1	62×10^4
4	0.1	114×10^4
5	0.04	101×10^4
6	0.01	78×10^4
7	0.01	72×10^4
8	0.001	78×10^4

Because plastic deformation is controlled by the effective stress, it is clear from the rate equation (Eqn. (1.7)) that small changes in τ_{eff} can cause a significant variation in the strain rate. In the present study it was found that in sintered iron the effective stress τ_{eff} is only 11% $\pm$ 3% of the applied stress τ_a. Consequently, the change

in the effective stress corresponding to the different strain rates is so small that it is masked by the random variation of the structure.

Because the behaviour varied in a random manner from one specimen to another, only one tensile test curve is shown. Fig. 3.12 shows the load as a function of elongation at a strain rate of 0.001/min. A yield effect was observed in one of the tests and is shown in Fig. 3.13. The figure shows part of the load-elongation curve measured at a strain rate of 0.1/min. The scatter observed in the tensile tests from one specimen to another explains why the stress relaxation tests varied considerably at the low stress levels.

Tensile tests were carried out by Krasovskii (34) on porous iron. He considers that the scatter in strength values may not be caused by the accidental scatter in porosity but is determined by the weakest cross section in the specimen. This may be caused by the non uniform compacting and sintering of the specimen. Artusio (35) and co-workers determined the effect of porosity and pore size on the elastic modulus of sintered iron. Their results indicate that the elastic modulus decreases with increasing porosity. At 13% porosity (6.8 g/cm^3 density) the elastic modulus is $\sim$ 70% of that of the wrought iron. In the present investigation, the slope of the stress-strain curve in the pre-yield was $\sim 85 \times 10^4$ kg/cm^2. The true dynamic elastic modulus can be expected to be $\sim$ 30% higher than this value. Thus $E \approx 110 \times 10^4$ kg/cm^2. This value is $\sim$ 55% of the elastic modulus of the wrought iron and it is in good agreement with $E \sim 120 \times 10^4$ kg/cm^2 measured by Andreotti and McGee (36) in sintered iron of 6.8 g/cm^3 density.

THE SERRATED YIELD EFFECT

In the course of tensile testing, a repeated yield effect or load fluctuation was observed as shown in Figs. 3.12, 3.13. Because no

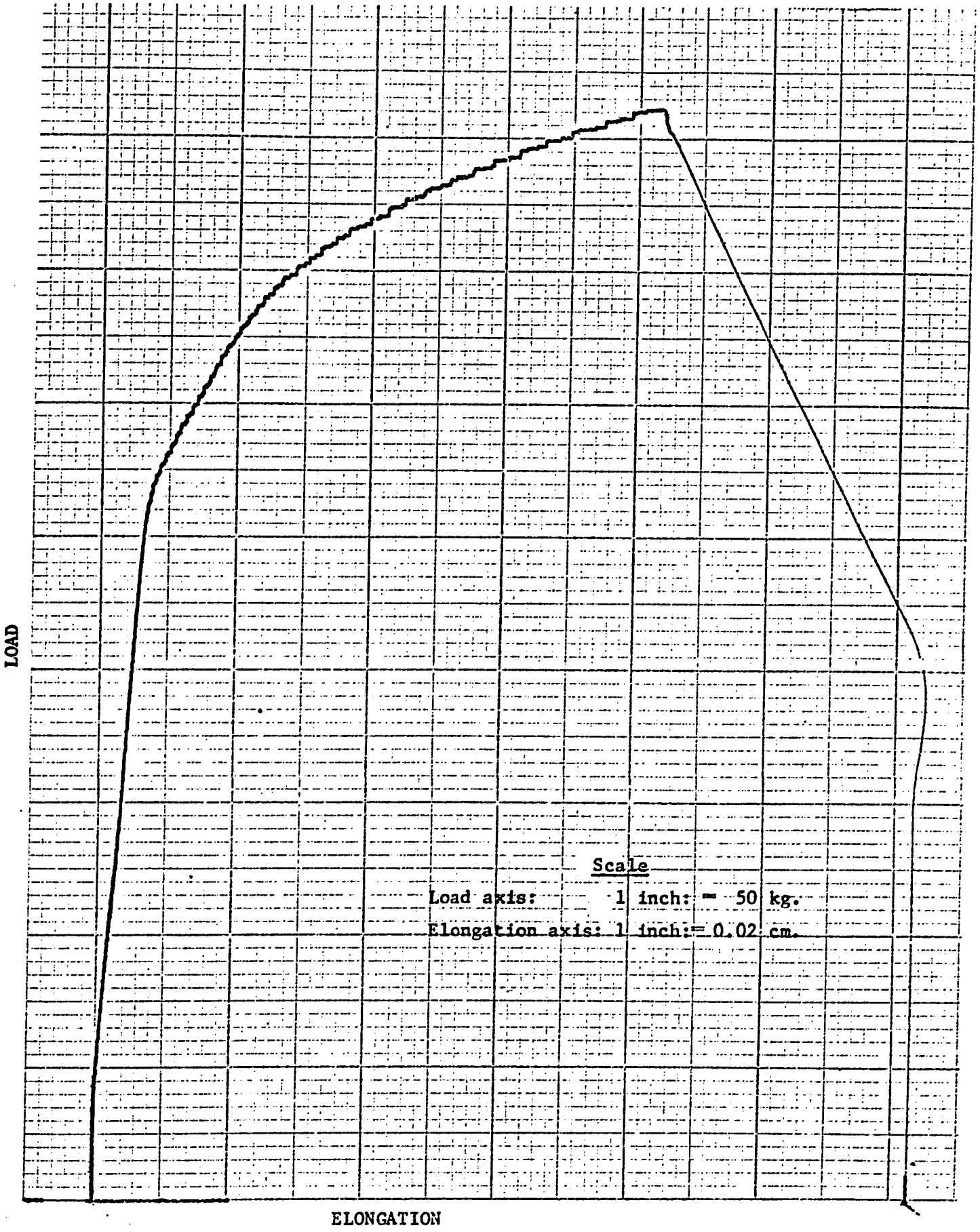

Fig. 3.12 The diagram shows the load-elongation curve for the sintered iron at a strain rate of 0.001/min.

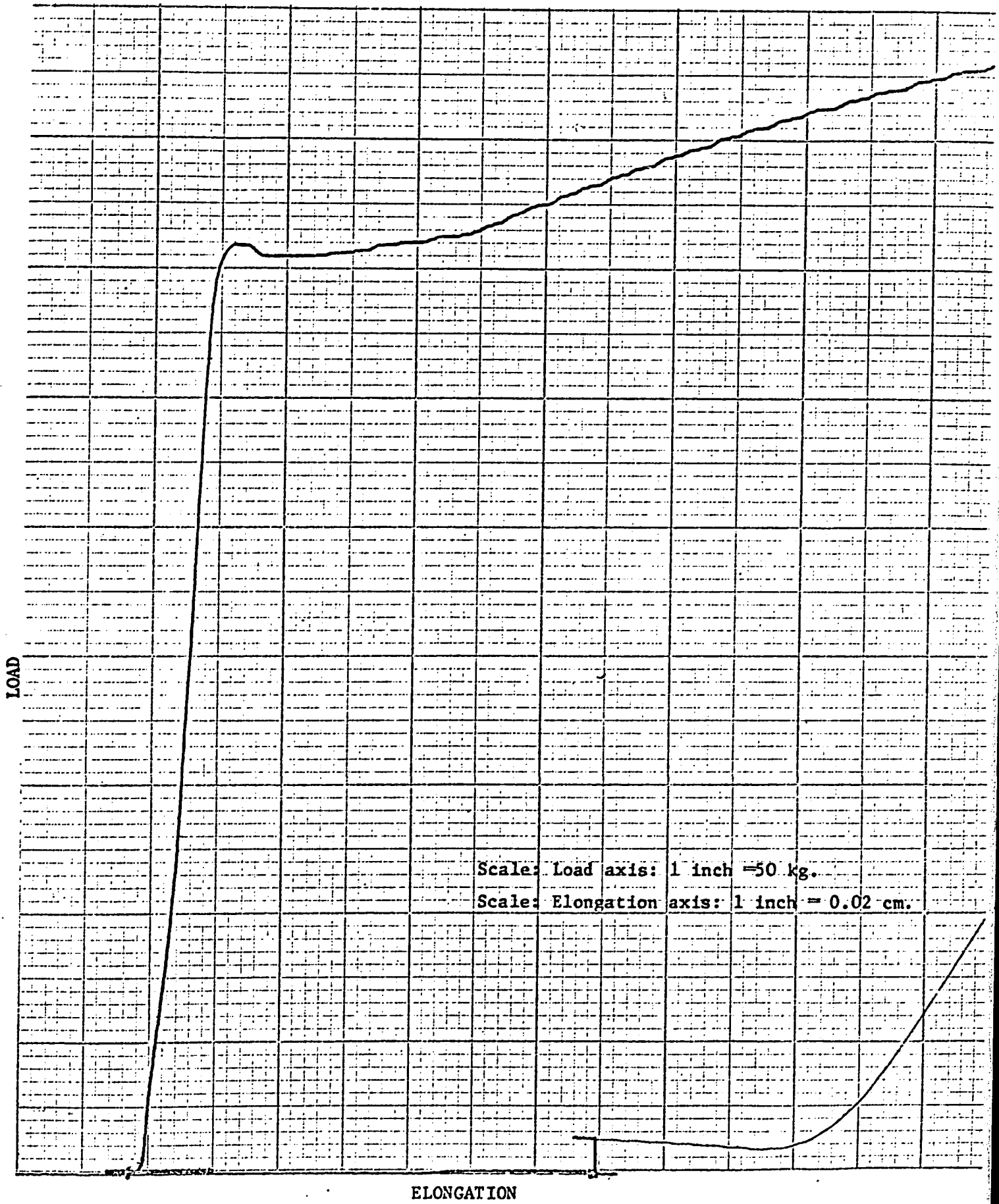

Fig. 3.13 The diagram shows part of the load-elongation curve measured at a strain rate of 0.1/min to illustrate the yield effect observed in sintered iron.

slip could occur in the grips used in these tests, it was concluded that the effect was real and it was decided that this infrequently observed phenomenon should also be investigated.

A similar effect was noted by Elam (37) in Al alloys and in Armco iron. Manjoine (38),in a series of tests on low carbon steel, observed load oscillations at 200° C and at strain rates of 2×10^{-2} sec^{-1} and 8.5×10^{-4} sec^{-1}. These oscillations occured only after 4 - 8% strain : Cottrell (39) found that the effect is absent in pure Al but could be observed in Al - Mg, and Al - Cu alloys. His studies showed that in iron with increasing strain rate, the effect is observable only at higher temperatures as shown in Table 3. 7. The table shows the lower temperature limit at which serrated yield could be observed at the indicated strain rates.

TABLE 3. 7
LOWER TEMPERATURE LIMIT FOR SERRATED YIELDING IN IRON

$\dot{\epsilon}$ sec^{-1}	4×10^{-5}	8.3×10^{-3}	5.0
T °K	330	410	620

The results of these experiments indicate that the process is thermally activated. Measurements (40, 41) show that the activation energy corresponds to that of the diffusion of N or C in iron.

A study by Mukherjee and co-workers (42) showed that in fully annealed 2074 Al alloy, the onset of repeated yielding was also a function of the strain rate and temperature. The activation energy was measured at the strain ϵ_o where the repeated yielding occured. The analysis was carried out with the rate equation

$$\dot{\epsilon} = A \epsilon_o^m \exp(-\Delta E_m / kT).$$

based on a model of impurity diffusion. The corresponding activation energy is calculated theoretically to be $\Delta E_{th} = 0.65$ ev in close agreement with the measured $\Delta E_m = 0.56 \pm 0.02$ ev.

All these observations were made on non sintered metals. The literature survey indicated that only one study was carried out in which repeated yield was observed in sintered iron. In this work (43) the effect of the finely dispersed CaO and MgO is carbonyl iron was investigated at room and at elevated temperatures. In the 150°C - 300° C region, repeated yield was observed. The results indicated that the effect was caused by the interaction of the dislocations with the interstitial atoms.

It is concluded therefore, that the serrated yield effect observed in the present tests is a thermally activated process. This conclusion is of interest in the cold and hot forming of sintered iron. When there is a repeated yield point, the work piece will deform nonuniformly in plastic deformation. In consequence, in open die forging, bending, or in similar operations the shape change may not be uniform. Orowan (44) has demonstrated that a metal which has a yield point, when bent, does not form a smooth curve but a polygon.

Comparison with the results of other investigators

The results of the present tests on sintered iron are compared with some of the investigations carried out on iron under comparable testing conditions. Table 3.8 gives the references and the results.

TABLE 3.8

COMPARISON OF THE RESULTS

Reference	Material Tested	Testing Method	T_o C°	n_f cm^2/kg	V_{b^3}	m	τ_{eff} Kg/cm^2	τ_{eff}/τ_a
Li(22)	High purity iron	Stress relaxation	-	.0115	-	-	113	0.10
Wilson & Garofalo(45)	High purity iron	Stress relaxation	25	.0233	128	-	-	-
Michalak(46)	High purity iron	Strain rate cycling	27	-	-	-	150	.25-1.0
McRickard (47)	Ferrovac iron	Stress relaxation	25	-	76.4	-	150	-
Johnston & Stein(48)	F_e-3% Si	Strain rate change	-	-	-	45-90	-	-
		Direct dislocation velocity measurement	-	-	-	40	-	-
Noble & Hull	F_e-3.25%Si	Stress relaxation	20	-	-	75-112	-	-
Present investigation	Sintered iron	Stress relaxation	24	.0677	370	67-286	130	.13

The above results indicate that the plastic properties of sintered iron determined in the present investigation are similar to the properties

of iron and F_e - 3% Si alloy at room temperature. Further tests at high temperatures are needed to compare the properties of sintered iron with the wrought iron.

4. CONCLUSIONS

The following conclusions were reached from the stress relaxation and tensile test results obtained in sintered iron.

1. The activation volume for the sintered iron is $\leq 370\ b^3$.

2. The probable rate controlling mechanism for the dislocation movement in sintered iron is either the intersection of dislocations or the overcoming of the impurity barriers.

3. In the later stage of stress relaxation, the two term rate equation is not sufficient to describe the stress relaxation process in sintered iron. The results indicate that a second rate controlling mechanism may be noticeable in this range.

4. It is suggested that the second rate controlling mechanism may be associated with the diffusion of interstitial atoms.

5. The internal stress in the sintered iron is $\simeq 89\% \pm 3\%$ of the applied stress.

6. The tensile tests carried out at various strain rates (0.001/min to 1.0/min) did not show any consistent change in the stress-strain characteristics of the sintered iron powder compact. This is in full agreement with the prediction made from the results of the internal stress measurement and is considered to be a good evidence in support of the experimental results and the theory.

7. At room temperature, the plastic properties of sintered iron are similar to that of iron and F_e - 3% Si alloy.

REFERENCES

1. _____ Steel, Oct. 7th, 77 (1968).
2. M. Feir, Mat. Design Eng., 63, 88 (1966)
3. G. Bianco, Powder Met., 9, 291 (1962).
4. _____ Automatic Machining, Jan., 8 (1971).
5. E. Orowan, Proc. Phys. Soc., 52, 8 (1940).
6. J. J. Gilman, W. G. Johnston, J. Appl. Phys., 30, 129 (1959).
7. R. Becker, Z. Physik, 26, 919 (1925).
8. A. H. Cottrell, An Introduction to Metallurgy, Edward Arnold Publishers, London, 67 (1968).
9. W. Kauzmann, Trans. A. I. M. E., 143, 57 (1941).
10. A. S. Krausz, Acta Met., 16, 897 (1968).
11. A. S. Krausz, Ph. D. Thesis, Univ. of Toronto, Ontario, (1964).
12. O. H. Wyatt, Proc. Phys. Soc. Lond. B., 66, 459 (1953).
13. A. H. Cottrell, J. Mech. and Phys. of Solids, 1, 53 (1952).
14. F. Guiu, P. L. Pratt, Phys. Stat. Sol., 6, 111 (1964).
15. P. Trouton, A. O. Rankine, Phil. Mag., 8, 538 (1904).
16. J. Boyd, A. S. T. M., 37, 218 (1937).
17. P. Feltham, Phil. Mag., 6, 259 (1961).
18. P. Feltham, Phys. Stat. Sol., 3, 1340 (1963).
19. G. A. Sargent, Acta Met., 14, 663 (1966).
20. G. A. Sargent, B. J. Shaw, Acta Met., 14, 909 (1966).

21. P. J. Wray, G. T. Horne, Phil. Mag., 13, 899 (1966).

22. J. C. M. Li, Can. J. Phys., 45, 493 (1967).

23. S. M. Ohr, Progress Report, U. S. Atomic Energy Commission, Jan., (1966).

24. R. W. Rohde, C. H. Pitt, J. Appl. Phys., 39, 3186 (1968).

25. P. Feltham, G. Lehmann, R. Moisel, Acta Met., 17, 1305 (1969).

26. A. S. Krausz, Scripta Met., 2, 615 (1968).

27. H. Conrad, J. Metals, July, 582 (1964).

28. S. R. MacEwen, O. A. Kupcis, B. Ramaswami, Scripta Met., 3, 441 (1969).

29. A. S. Krausz, Mater. Sci. Eng., 4, 193 (1969).

30. A. S. Krausz, Can. J. Phys., 41, 167 (1963).

31. A. S. Krausz, To be published.

32. J. Friedel, Dislocations, Pergamon Press, Oxford, 454 (1964).

33. P. G. Shewmon, Diffusion in Solids, McGraw-Hill, N. Y., 88 (1963).

34. A. Ya. Krasovskii, The Eng. Index, 64, 1859 (1965).

35. G. Artusio, V. Gallina, G. Mannone, E. Sgambetterra, Powder Met., 9, 89 (1966).

36. E. R. Andreotti, S. W. McGee, Metal Prog., 89, 82 (1966).

37. C. F. Elam, Proc. Roy. Soc. London. A., 165, 568 (1938).

38. M. J. Manjoine, J. Appl. Mech., 11, 211 (1944).

39. A. H. Cottrell, Vacancies and other point defects in metals and alloys, Institute of Metals, London, 1 (1958).

40. J. Baruch, A. Rosen, S. R. Bodner, Trans. J. I. M., 9, 448 (1968).

41. A. Rosen, S. R. Bodner, Mater. Sci. Eng., 4, 115 (1969).

42. K. Mukherjee, T. May, R. J. Maciag, C. D'Antonio, Mater. Sci. Eng., 6, 334 (1970).

43. G. Schoenbauer, R. Mitsche, F. Benesovsky, The Eng. Index, 67, 2407 (1968).

44. F. R. N. Nabarro, Theory of Crystal Dislocations, Oxford, 398 (1967).

45. J. F. Wilson, G. F. Garofalo, Materials Research and Standards, 6, 85 (1966).

46. J. T. Michalak, Acta Met., 13, 213 (1965).

47. S. B. McRickard, Acta Met., 16, 969 (1968).

48. W. G. Johnston, D. F. Stein, Acta Met., 11, 317 (1963).

49. F. W. Noble, D. Hull, Acta Met., 12, 1089 (1964).